Earth-Science Reviews 243 (2023) 104501

Contents lists available at ScienceDirect

Earth-Science Reviews

journal homepage: www.elsevier.com/locate/earscirev

Advances in Earth observation and machine learning for quantifying blue carbon

Tien Dat Pham [a,*], Nam Thang Ha [b], Neil Saintilan [a], Andrew Skidmore [a,c], Duong Cao Phan [d], Nga Nhu Le [e], Hung Luu Viet [f], Wataru Takeuchi [g], Daniel A. Friess [h]

[a] School of Natural Sciences, Macquarie University, Sydney, NSW 2109, Australia
[b] Faculty of Fisheries, University of Agriculture and Forestry, Hue University, Hue 530000, Viet Nam
[c] Faculty of Geo-Information Science and Earth Observation (ITC), University of Twente, Enschede, the Netherlands
[d] Centre for AI and Applied Data Analytics, School of Computer Science, University of Dublin, Belfield, Dublin 4, Ireland
[e] Department of Marine Mechanics and Environment, Institute of Mechanics, Vietnam Academy of Science and Technology (VAST), Ba Dinh, Hanoi 100000, Viet Nam
[f] Centre of Multidisciplinary Integrated Technologies for Field Monitoring (FIMO), the University of Engineering and Technology, Vietnam National University (VNU), 144 Xuan Thuy, Cau Giay, Hanoi 100000, Viet Nam
[g] Institute of Industrial Science, the University of Tokyo, 4-6-1 Komaba, Meguro-ku, Tokyo 153-8505, Japan
[h] Department of Earth and Environmental Sciences, Tulane University, New Orleans, LA 70118, USA

ARTICLE INFO

Keywords:
Blue Carbon
Mangrove
Seagrass
Saltmarsh
Machine learning
Earth observation
Deep learning
Optimisation

ABSTRACT

Blue carbon ecosystems (mangroves, seagrasses and saltmarshes) are highly productive coastal habitats, and are considered some of the most carbon-dense ecosystems on Earth. They are an important nature-based solution for both climate change mitigation and adaptation. Quantifying blue carbon stocks and assessing their dynamics at large scales through remote sensing remains challenging due to difficulties of cloud coverage, spectral, spatial and temporal limitations of multispectral sensors and speckle noise of synthetic aperture radar (SAR). Recent advances in airborne and space-borne multispectral and SAR imagery and Light Detection and Ranging (LiDAR) data, sensor platforms such as unmanned aerial vehicles (UAVs), combined with novel machine learning techniques have offered different users with a wide-range of spectral, spatial, and multi-temporal information for quantifying blue carbon from space. However, a large number of challenges are posed by various traits such as atmospheric correction, water penetration, and water column transparency issues in coastal environments, the multi-dimensionality and size of the multispectral and LiDAR data, the limitation of training samples, and backscattering mechanisms of SAR imagery in the acquisition process. As a result, existing methodologies face major difficulties in accurately estimating blue carbon stocks using these datasets. In this context, emerging and innovative machine learning and artificial intelligence methodologies are often required for robustness and reliability of blue carbon estimates, particularly those using open-source software for signal processing and regression tasks. This review provides an overview of Earth Observation data, machine learning and state-of-the-art deep learning techniques that are currently being used to quantify above-ground carbon, below-ground carbon, and soil carbon stocks of mangroves, seagrasses and saltmarshes ecosystems. Some key limitations and future directions for the potential use of data fusion combined with advanced machine learning, deep learning, and metaheuristic optimisation techniques for quantifying blue carbon stocks are also highlighted. In summary, the quantification of blue carbon using remote sensing and machine learning approaches holds great potential in contributing to global efforts towards mitigating climate change and protecting coastal ecosystems.

1. Introduction

Blue carbon ecosystems consist of mangroves, saltmarshes, and seagrasses, which sequester carbon within their above-ground biomass (AGB) and below-ground biomass (BGB), and ultimately store it in their sediments (Donato et al., 2011; Macreadie et al., 2019). Blue carbon ecosystems are highly productive coastal habitats and are considered some of the most carbon-dense ecosystems on the earth; on average,

* Corresponding author.
E-mail address: tiendat.pham@mq.edu.au (T.D. Pham).

https://doi.org/10.1016/j.earscirev.2023.104501
Received 30 May 2022; Received in revised form 27 June 2023; Accepted 5 July 2023
Available online 13 July 2023

mangroves may store two to four times more carbon per unit area than terrestrial forests (Donato et al., 2011), while seagrass meadows can store twice as much per unit area (Fourqurean et al., 2012). The total area of blue carbon ecosystems is estimated to be approximately 185 million ha, storing more than 30,000 Tg C across their range (Macreadie et al., 2021).

Mangrove forests have the highest climate change mitigation potential of all blue carbon ecosystems (726 Tg CO_2-e yr^{-1} from avoided habitat loss and restoration) due to their high carbon densities, scale of loss, and biophysical potential for restoration (Macreadie et al., 2021). Mangrove forests covered approximately from 140,260 to 152,000 km^2 in 2020 (Bunting et al., 2022) along tropical, subtropical and warm temperate coastlines. One-third of the world's mangroves have been destroyed over the past 65 years in a wide ranges of climatic regions. However, a lower rate of mangrove loss has been observed in the 21st Century, as a result of changing agricultural practices coupled with increased conservation and restoration of mangroves, in part because of the growing recognition of their role in climate change mitigation (Friess et al., 2019). Saltmarshes are salt-tolerant herbaceous plants found across tropical, sub-tropical and temperate inter-tidal zones, covering an estimated from 44,000 to 55,000 km^2 (Murray et al., 2022). Saltmarshes have been lost due to land development and reclamation, dredging and coastline transgression (Prahalad et al., 2020; Rogers and Krauss, 2019; Saintilan et al., 2014), and avoiding further habitat loss coupled with restoration of damaged areas has a climate change mitigation potential of 78 Tg CO_2-e yr^{-1} (Macreadie et al., 2021). Seagrasses represent 76 species of submerged monocotyledonous and flowering plants, with a near global distribution (Fourqurean et al., 2012). Estimates of their extent range from 16,000 to 165,000 km^2 (Jayathilake and Costello, 2018; McKenzie et al., 2020), though continue to show rapid decline with a net loss of 5602 km^2 (Dunic et al., 2021). As such, their avoided habitat loss and restoration could lead to a climate change mitigation potential of 341 Tg CO_2-e yr^{-1} (Macreadie et al., 2021).

Earth observation (EO) datasets have been proven to be suitable for effective monitoring of ecosystems, and specifically blue carbon ecosystems, as they offer lower costs, reliable information on vegetation, and cover large areas (Campbell et al., 2022; Farzanmanesh et al., 2021; Pham et al., 2019a; Pham et al., 2019b). Mangrove forests and saltmarshes in particular can be effectively mapped using remote sensing as their canopies emerge above the water surface, making them visible from space. During the last decade, the rapid development of computer science, artificial intelligence, and satellite infrastructure has also facilitated the development of toolsets and new methods for the estimation of blue carbon from space (Beyan and Browman, 2020; Zhang et al., 2021). Recent advances in geospatial technologies using multi-sensor and multi-temporal space-borne satellite data fusion approaches including the integrating multispectral and synthetic aperture radar (SAR) data and air-borne LiDAR data with advanced machine learning and metaheuristic optimisation techniques (Lausch et al., 2022; Pham et al., 2021) are also beginning to be used in blue carbon mapping.

While it is now common practice to monitor blue carbon ecosystems across large scales using remote sensing, some challenges exist to mapping all ecosystems. Limitations discussed in the literature include cloud coverage constraints for passive sensors, the limited training samples for monitoring mangroves and saltmarshes (Farzanmanesh et al., 2021; Pham et al., 2019a) and seagrass meadow dynamics (Veettil et al., 2020). Furthermore, the characteristics of each ecosystem require different remote sensing approaches. Mangroves and saltmarshes differ from seagrasses in their location in the intertidal zone, as well as their morphological characteristics, both of which provide challenges to habitat mapping. Mangroves and saltmarshes are found at higher elevations, and the mangrove canopy is often fully above from the water column, while saltmarshes will be exposed for lengthy periods. However, seagrass is found in the lower inter-tidal and upper sub-tidal zones, so are covered by water for longer periods, hampering the mapping of seagrass under water and requiring additional processing of satellite images to map the meadow's spatial distribution. In most cases, the majority of the seagrass meadow remains submerged even on the lowest low tides. In some cases, seagrass meadows are exposed to the air during extreme low tides, however it is challenging to ensure overlapping of the low tide time and the satellite acquisition date, which is required to reduce the effect of the water column on the image pixel. Remote sensing is particularly challenging for seagrasses, which can have different spectral characteristics depending on their species/growth form, age, and depth. This can make them challenging to accurately map seagrasses using remote sensing data, especially when different species of seagrasses are present in the same area. Seagrass distribution and extent can also be influenced by environmental conditions such as water quality, temperature, salinity, and wave exposure. These factors can vary greatly between different locations and over time, which can affect the accuracy of seagrass mapping using EO data (Lebrasse et al., 2022a; Lebrasse et al., 2022b). Thus, accurate estimates of seagrasses are limited due to the diverse difference associated with their location, limitations of mapping techniques and insufficient ground reference data (McKenzie et al., 2020; Unsworth et al., 2019), resulting in uncertainty of seagrass blue carbon estimation. This highlights the need for improved availability of source data for validation of the global datasets, and it requires additional effort to be made in developing advanced mapping techniques and fostering collaboration to improve the certainty and accuracy of seagrass carbon estimation.

This review provides a critical overview of the use of numerous remote sensing approaches, machine learning and state-of-the-art deep learning techniques to quantify above-ground carbon (AGC), below-ground carbon (BGC), and soil carbon stocks of blue carbon ecosystems. This review addresses the capability of various remote sensing approaches for quantifying mangrove blue carbon and monitoring their dynamics, and the limitations of the use of SAR and LiDAR sensors for quantifying submerged seagrass and saltmarshes. We also highlight a number of key future directions and the potential application of multi-source, multi-sensor, and multimodal remote sensing data, advanced machine learning, deep learning, and metaheuristic optimisation techniques for quantifying blue carbon stocks.

2. Remote sensing approaches for blue carbon estimates

Field-based in-situ measurements or ground-truth data are required to develop regression models for quantifying blue carbon from remote sensing, and to assess the accuracy of models using various EO datasets highlighted in this section. In-situ sampling plots geo-located using handheld GPS are often established to collect data on the community structure of blue carbon ecosystems. These may include biomass measurements such as Diameter of Breast Height (DBH) and tree height (H), which are required for calculating mangrove AGB using allometric equations (Komiyama et al., 2008). Saltmarsh AGB is clipped within subplots of size 0.5 m × 0.5 m, and fresh biomass is subsequently measured using a digital weighing scale. Based on these subplot measurements, the average fresh and dry weight AGB per plot is calculated (Rasel et al., 2019).

A 0.5 m × 0.5 m square quadrat and a plastic core are used to collect seagrass and measure the dry weight AGB. Three cores are used in each plot, and all shoots within the plastic core, with a diameter of 15 cm and a depth of 40 cm, are collected. The seagrass samples are stored in a labelled plastic bag. The seagrass AGB is left in the oven and dried at 60 °C for 48 h. After that, the seagrass samples are taken out of the oven, cooled to room temperature, and instantly weighted (Fourqurean et al., 2012). The seagrass AGB is measured in gram of dried weight per square metre (g DW m^{-2}).

Numerous research studies have employed various airborne and space-borne hyperspectral, multi-spectral sensors and LiDAR as well as an Unmanned Aerial Vehicle (UAV) platforms for quantifying blue carbon and monitoring their carbon dynamics.

Fig. 1 shows the remote sensing approaches that have been used for

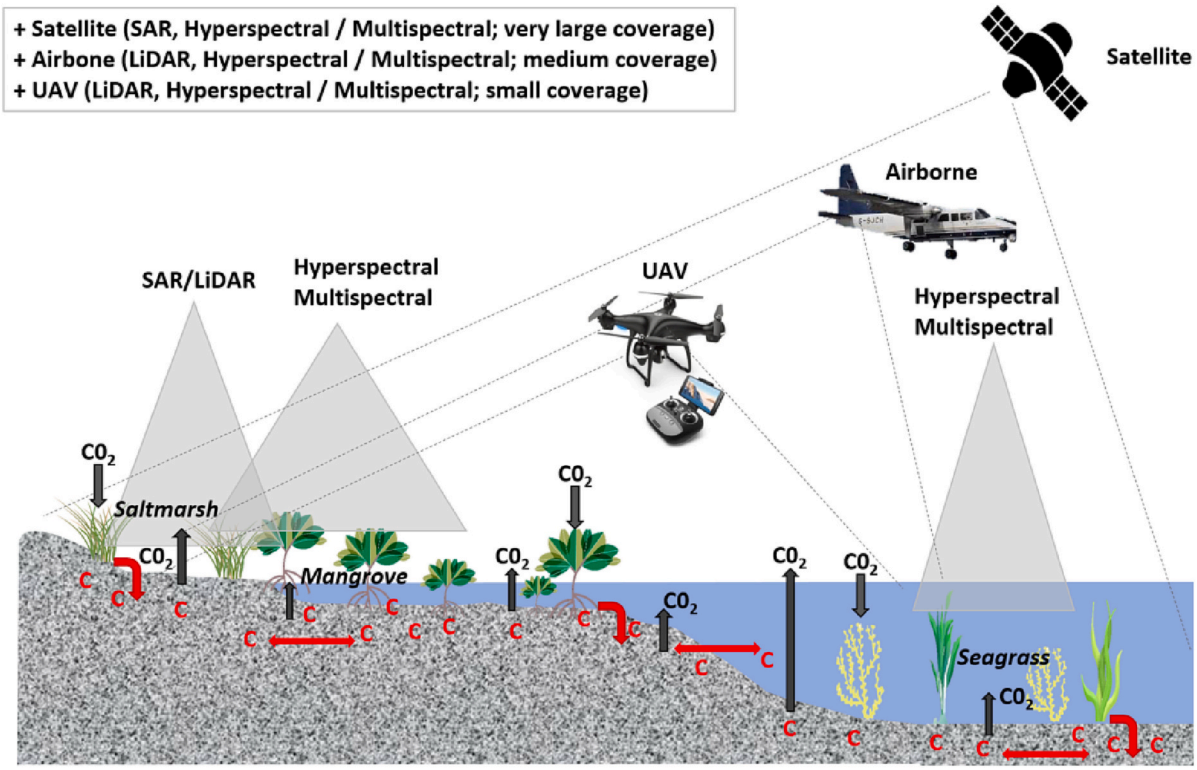

Fig. 1. Remote sensing approaches used for quantifying blue carbon and monitoring their carbon change.

quantifying blue carbon and monitoring their carbon changes.

Remote sensing approaches can be broadly divided into space-borne, air-borne sensors, and the Unmanned Aerial Vehicle (UAV) systems. Satellite sensors include hyperspectral imaging, multispectral and Synthetic Aperture Radar (SAR) data, which generally can cover large areas. Airborne sensors, which consisted of hyperspectral, multispectral, and LiDAR data, may only cover relatively small regions whereas the UAV systems are only able to capture limited areas (Table 1).

It is important to note that several satellite missions, including Hyperion, Landsat-7 and earlier, SPOT-4 and SPOT-5, Rapid Eye and ALOS AVNIR-2 are no longer operational.

2.1. Multispectral data

Multispectral sensors utilize the visual, near-infrared, and short-wave infrared electromagnetic spectrum for locating and monitoring the condition of objects (Jensen, 1996). Objects made of different materials absorb and reflect light differently across multiple wavelengths or bands. Multispectral remote sensing technology takes advantage of these unique spectral signatures to identify and distinguish between different objects or features. One of the most important series of multispectral remote sensing satellites has been the multispectral Land Remote-Sensing Satellite (the Landsat program) (Wulder et al., 2019). This project has provided a large number of long-term multispectral datasets over multiple decades. Landsat data have been used in numerous studies in the environmental field, including land use/land cover dynamic analysis (Duong et al., 2018; Phan et al., 2021a), forest change (Truong et al., 2019; Zheng and Takeuchi, 2020; Zheng and Takeuchi, 2022), flood susceptibility mapping (Ngo et al., 2021; Nhu et al., 2020), among others. In recent years, multispectral data have been commonly used in various practical applications including the estimations of blue carbon stocks (Pham et al., 2019a; Table 1).

The increasing advancement of multispectral satellites has developed finer spatial-temporal resolution (0.5–5.0 m) satellite sensors such as SPOT, Quickbird, WorldView, RapidEye, IKONOS, PlanetScope and OrbView. These optical sensors have recently been utilised to map and quantify blue carbon in mangrove and saltmarsh ecosystems, owing to their improved spatial, temporal, and spectral resolutions (Warwick-Champion et al., 2022). In addition, airborne sensors have been widely developed, for example, the Leica Geosystems ADS-40 and Z/I Digital Modular Camera (DMC) (Apostolopoulos and Nikolakopoulos, 2021). These sensors provide higher resolutions than many previous multispectral sensors as they are based on airborne platforms that can fly closer to the landscape of interest. However, these sensors are rarely radiometrically calibrated, resulting in problems in terms of absolute quantification of standing biomass, automated processing and image-to-image reliability. Thus, they are less often used for quantifying blue carbon compared to freely available satellite data sources, due to cost and limited coverage.

Prior research has shown that optical remote sensing data have become a well-known means of blue carbon assessments, especially the estimations of leaf chlorophyll and leaf area index (LAI) (Franklin and Miller, 2010). For example, Ha et al. (2021a) used Landsat images at 30-m spatial resolution to detect changes in seagrass species in Tauranga Harbour, New Zealand. Although Landsat was able to successfully estimate long-term changes in seagrass cover, its moderate spatial-temporal resolution (30 m and 16-day repeat coverage) posed challenges in accurately estimating changes in the intertidal zones, which are more variable over time. To handle such a problem, finer spatial-temporal resolution datasets such as Sentinel-2 multispectral instrument (MSI) and ALOS AVNIR-2 sensor with a spatial resolution of 10 m have been employed to improve blue carbon stock assessments (Méléder et al., 2020). Sentinel-2 MSI data recently have been widely used to quantify blue carbon in mangroves (Rijal et al., 2023), in seagrass meadows (Ha et al., 2023; Nabil Akbar et al., 2021) and saltmarshes (Ladd et al., 2022). Several attempts have been made to estimate carbon stocks stored in coastal and marine ecosystems by utilizing very high spatial resolution multispectral images such as Planet Scope (~ 3 m) and WorldView (~2 m) sensors (Coffer et al., 2020; Csillik et al., 2019). Interestingly, the Planet constellation of Earth observing satellites offer

Table 1
Summary of remote sensing data used for quantifying blue carbon and monitoring their change.

BC ecosystem	Dataset								Location
Mangrove	**HS**		**MS**		**SAR**		**LiDAR**	**UAV**	
	Sensor	Spatial resolution	Sensor	Spatial resolution	Sensor	Spatial resolution			
Anne et al. (2014)	Hyperion	30							Florida, USA
Shapiro et al. (2015)			Landsat-7 ETM+ and Landdsat-8 OLI	30	SRTM	30	√		Zambezi Delta, Mozambique
Dube and Mutanga (2015)			Landsat-8 OLI	30					South Africa
Wicaksono et al. (2016)			ALOS AVNIR-2	10					Karimunjawa, Indonesia
Maeda et al. (2016)			Rapid Eye	5			√		South Sumatra, Indonesia
Pham et al. (2017)					ALOS-2 PALSAR-2	6.5			Hai Phong city, Vietnam
Pham and Brabyn (2017)			SPOT-4 and SPOT-5	10					Can Gio, Vietnam
Benson et al. (2017)			Landsat-7 ETM+ and Landsat-8 OLI	30					Southwest Madagascar
Hickey et al. (2018)			Landsat-8 OLI				√		Northern Western Australia
Bolivar et al. (2018)			MODIS	250					Colombia
Omar et al. (2018)			Landsat-5 TM and Landsat-7 ETM+	30					Malaysia
Sanderman et al. (2018)			Landsat-5 TM	30					Global
Hamilton and Friess (2018)			Landsat-5 TM and Landsat-8 OLI	30					Global
Simard et al. (2019)					SRTM	30	√		Global
Lagomasino et al. (2019)			Landsat-8 OLI	30	Sentinel-1 and TerraSAR-X	10 4			
Li et al. (2019)								√	Shenzhen Bay, China
Anand et al. (2020)	Hyperion	30							Odisha, India
Bindu et al. (2020)			LISS-IV	5.8					Kunhimangala, India
Suyadi et al. (2020)			Landsat-5 TM	30			√		Auckland, New Zealand
Trettin et al. (2021)					Tan DEM-X	4			Gabon, Africa
Pham et al. (2021a)			Sentinel-2A and Sentinel-2B	10					North Vietnam
Rijal et al. (2023)			Sentinel-2B and Sentinel-1B	10					Komodo National Park, Indonesia
Seagrass									
Hill et al. (2014)	Airborne Spectroscopic Aerial Mapping System with On-board Navigation (SAMSON)	1							Saint Joseph's Bay, Florida, USA
Isnaen et al. (2019)			Planet Scope	3					Sumatra, Indonesia
Nabil Akbar et al. (2021)			Sentinel-2A	10					Sulawesi, Indonesia
Lebrasse et al. (2022a)			Landsat-5 TM and Landsat-8 OLI	30					Florida, USA
Ha et al. (2023)			Sentinel-2 and Sentinel-1	10					Tauranga Harbour, New Zealand
Saltmarsh									
Kulawardhana et al. (2014)			Aerial photographs				√		Galveston Island, Texas, USA
Byrd et al. (2018)			Landsat-5 TM, Landsat-7 ETM+ Landsat-8 OLI	30	Sentinel-1	10			United States (CONUS)
Sejati et al. (2020)			Landsat-8 OLI	30	Sentinel-2A	10			Indonesia

(*continued on next page*)

Table 1 (*continued*)

BC ecosystem	Dataset								Location
Mangrove	HS		MS		SAR		LiDAR	UAV	
	Sensor	Spatial resolution	Sensor	Spatial resolution	Sensor	Spatial resolution			
Ladd et al. (2022)			Sentinel-2	10					Skinflats and Caerlaverock in Scotland
Chen et al. (2022)			Sentinel-2	10					Shandong Province, China
Warwick-Champion et al. (2022)			Planet Scope	3					Jervis Bay, New South Wales, Australia
Tang et al. (2022)					UAV-LiDAR	0.05	√	√	Yangtze River Estuary, China

Note: HS: Hyperspectral; MS: Multispectral.

to freely access data of Planet Imagery up to 5000 km^2 monthly via Education and Research program (https://www.planet.com/markets/education-and-research/). Recent studies attempted to map seagrass carbon in Indonesia (Isnaen et al., 2019) and saltmarsh carbon in Australia (Warwick-Champion et al., 2022). However, multispectral optical data frequently face limitations such as high-frequent cloud cover in tropical zones, their operation during daytime only, and the attenuation of the signal in multispectral bands in the water column, which has been a challenge when mapping habitat in submerged aquatic environments (Hedley et al., 2012; Sani et al., 2019).

One potential remote sensing approach to address these issues is to combine optical data with active remote sensing data from instruments such as Synthetic Aperture Radar (SAR) or Light Detection and Ranging (LiDAR). For example, ALOS-2 PALSAR-2 and Sentinel-2 data have been fused to estimate mangrove aboveground biomass in a tropical dense cloud-cover area in Vietnam (Pham et al., 2018). Likewise, Kulawardhana et al. (2014) employed a combination of LiDAR and multispectral data to estimate the AGB and carbon stocks of saltmarshes using allometric relations and transfer coefficients in the West Galveston Bay on Galveston Island, in the United States.

2.2. Hyperspectral imaging

Hyperspectral sensors offer valuable information for blue carbon estimations by providing a high spectral resolution and a wide range of wavelengths. Compared to multispectral imaging, hyper-spectral sensors quantify a larger number of continuous narrow spectral bands (Hagen and Kudenov, 2013). Hyperspectral imaging often utilizes a range of wavelengths between 380 and 2500 nm, with a narrow bandwidth of less than 10 nm. These advanced characteristics make hyperspectral imagery more useful than traditional multispectral data. Previous research has demonstrated that the use of hyperspectral data for monitoring mangrove biomass and blue carbon stocks results in more accurate estimates than the utilisation of multispectral data, such as Landsat and SPOT(Anand et al., 2020; Pandey et al., 2019). One possible reason for hyperspectral sensors being more useful than multispectral sensors for carbon quantification is that they can collect a large number of narrow and contiguous spectral bands, providing more detailed spectral information compared to the fewer and broader spectral bands of multispectral sensors. This allows hyperspectral sensors to better distinguish between different types of vegetation and accurately estimate vegetation properties such as biomass and carbon content. Additionally, hyperspectral sensors offer higher spectral information and a greater signal-to-noise ratio than multispectral sensors, which can further improve the accuracy of carbon estimations. However, hyperspectral sensors such as Hyperion, DESIS (German Aerospace Center Earth Sensing Imaging Spectrometer), PRISMA (PRecursore IperSpettrale della Missione Applicativa), TianGong-1, EnMAP (Environmental Mapping and Analysis Program), HyspIRI (Hyperspectral Infrared Imager), and HISUI (Hyperspectral Imager SUIte) have drawbacks associated with a limited coverage (Transon et al., 2018) in comparison to other data types. However, some studies have used the Hyperion sensor to quantify mangrove and seagrass carbon stocks (Anand et al., 2020; Anne et al., 2014). For example, Hill et al. (2014) highlight the ability of a high spatial resolution (~ 1 m) airborne hyperspectral sensor to quantify seagrass biomass and productivity in Florida, USA (Table 1). Hyperspectral imaging may become more commonly used as UAV system-based hyper-spectral sensors become available that are able to offer a wide range of wavelengths from 400 to 2500 nm, which may be useful for soil carbon estimates of blue carbon ecosystems. The operation of current hyper-spectral imaging projects, such as the EnMap, the PRISMA, and the HISUI missions is a great opportunity for blue carbon quantification in the near future (Transon et al., 2018).

2.3. Synthetic Aperture Radar (SAR)

SAR adopts an active microwave imaging technique to observe objects from a remote distance, and offers several advantages over optical remote sensing (Bamler, 2000). For example, SAR actively uses its own energy and thus is not dependent on sunlight brightness, so is not restricted to data collection during daylight hours. SAR utilizes microwave wavelengths (0.2–100.0 cm) that are able to penetrate certain materials such as clouds and the forest canopy. However, microwave radiation is strongly attenuated by liquid water, rendering this technology unusable for the remote sensing of submerged vegetation. The most widely used SAR sensors including Sentinel-1, ERS-1 and 2, ENVISAT, ALOS PALSAR, ALOS-2 PALSAR-2, TerraSAR-X, COSMO-SkyMed, RADARSAT-2. They have been widely employed for various utilizations such as deforestation and degradation monitoring of forests (Mansfeld and Runia, 2010), land use/land cover assessments (Phan et al., 2021b), flash-flood hazard prediction (Ngo et al., 2021), and the identification of urban objects (Kumar, 2021).

It is possible that SAR with different wavelengths (referred to as bands or designated letters such as Ka, K, Ku, X, C, S, L, and P) gives additional benefits in the estimation of carbon stocks of mangrove forests (Fig. 2). For example, the wavelengths of the X-band (3.8–2.4 cm) rarely penetrate deeply into vegetation cover and thus can be used to monitor canopy surfaces. Longer wavelengths (e.g. L-band: 24 cm) can go through leaves into stems and branches, which are frequently adopted for the measurements of species structures (Englhart et al., 2011). SAR sensors also commonly use horizontal (H) and vertical (V) polarizations. Particularly, HV indicates signals emitted in horizontal and received in vertical polarization. Different polarizations can be used to distinguish characteristics of targeted objects. For example, VV scattering is most sensitive to rough surfaces while VH and HV are most sensitive to the branches and leaves of a forest canopy (Darmawan et al., 2019; Pham and Yoshino, 2017; Pham et al., 2017). These characteristics of SAR data have made these sensors increasingly popular for the

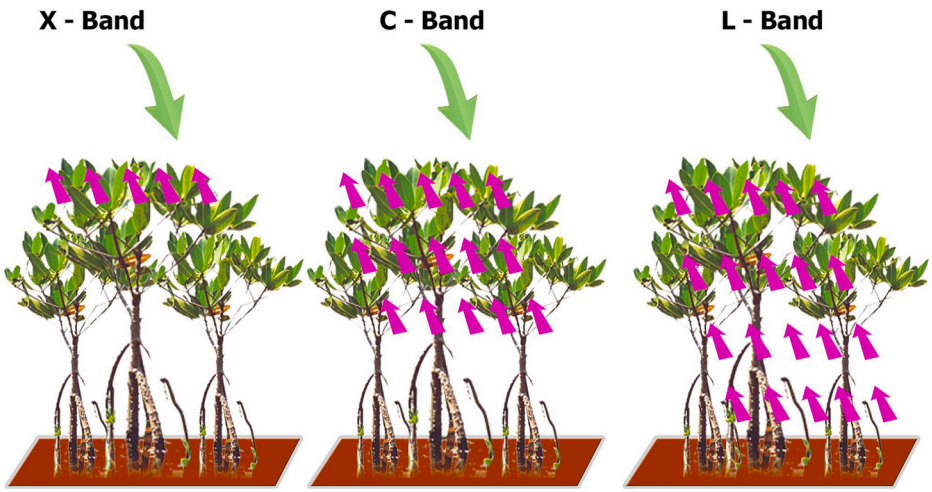

Fig. 2. Wavelengths of radar system through mangrove forests. Source: modified from the European Space Agency (ESA) as cited in Pham et al. (2019b).

quantification of mangrove forests. For example, Thomas et al. (2015) demonstrated the potential of time-series JERS-1 SAR and ALOS PALSAR datasets for mapping mangrove extent. However, relatively few studies have gone beyond areal extent mapping and applied SAR data to the assessment blue carbon stocks (Table 1). Where SAR has been used for blue carbon quantification, it has often been integrated with multispectral data, which can outperform the use of SAR data alone (Sinha et al., 2015). SAR approaches are not commonly used to map submerged seagrasses as the SAR band energy penetrates only a few cm into the water before it is completely absorbed and may not be useful for submerged plant canopy from the bottom. However, some intertidal populations of seagrasses exposed at low tide can be mapped using diffusely elevated backscatter values from SAR, due to some levels of surface roughness created by the seagrass vegetation (Veettil et al., 2020). This has been shown to improve the accuracy of seagrass mapping and AGB estimates (Simpson et al., 2020).

2.4. LiDAR

Light Detection and Ranging (LiDAR) is another active remote sensing approach that can provide highly accurate and detailed measurements of vegetation height and structure, which are important indicators of carbon stocks in ecosystems such as mangroves and saltmarshes. Some LiDAR sensors also have the ability to penetrate through vegetation canopies and map the underlying terrain, allowing for the creation of digital elevation models that can be used to estimate the volume of sediment and carbon stored in coastal ecosystems. LiDAR has been commercially applied to topographic and bathymetric fields since the mid-1990s (Yan et al., 2015) and to map aspects of mangroves and saltmarshes (e.g., Friess et al., 2014; Owers et al., 2018). LiDAR differs from SAR by utilising shorter wavelengths than the microwaves applied in SAR. Specifically, while near-infrared light is usually adopted for topographic applications, water-penetrating green light is typically used for bathymetric purposes. In comparison with 2D remotely sensed data, a LiDAR sensor can measure the 3D topographic profile of surfaces. It has other advantages such as penetration of tree canopy, without affecting relief displacement, shadowing, and lighting conditions. LiDAR is frequently used on an airborne platform, though spaceborne LiDAR has begun to be used in multi-sensor approaches to quantifying forest height and AGB (Potapov et al., 2021). LiDAR has been commonly used to create digital elevation models (DEM) and shoreline maps, used for land use/land cover monitoring (Qin et al., 2016), mangrove species classification (Cao et al., 2021) and tree canopy height estimation (Feliciano et al., 2017).

LiDAR has been increasingly used to generate blue carbon estimates in mangroves (Pham et al., 2019a) and saltmarshes (Kulawardhana et al., 2014; Tang et al., 2022; Table 1). For instance, Wannasiri et al. (2013) used airborne LiDAR to extract the biophysical parameters of mangroves on the coast of Thailand, showing that LiDAR is of potential use for estimating the position, height, and crown diameter of individual trees. Spaceborne LiDAR also has applications in blue carbon mapping; ICE Sat/GLAS data have been widely used to estimate global mangrove canopy heights (Simard et al., 2019; Simard et al., 2006), from which mangrove carbon stocks can then be estimated. The NASA's Global Ecosystem Dynamics Investigation (GEDI) LiDAR has begun to be used for canopy height estimates in mangrove forests, and have shown improved accuracies when fused with radar sensors (Stovall et al., 2021). Nevertheless, there are several limitations of LiDAR sensing. For example, LiDAR faces challenges in accurately measuring dense tree crowns (Wannasiri et al., 2013). LiDAR data alone cannot provide sufficiently accurate estimates of biomass and carbon stocks in blue carbon ecosystems due to the limited sensitivity to submerged vegetation and the complex structures associated with tides and water levels (Hudak et al., 2012). Hence, the integration of LiDAR with other remote sensing data such as multispectral data and SAR data is recommended for accurate mangrove biomass and carbon assessment (Pham et al., 2019a; Sani et al., 2019). For instance, Tang et al. (2022) used UAV-based LiDAR to map the spatial distribution of saltmarsh communities and their AGB in China, whereas Kulawardhana et al. (2014) fused LiDAR and multispectral data to quantify saltmarsh carbon stocks in West Galveston Bay, Texas in the US.

2.5. UAVs platforms

The term "Unmanned Aerial Vehicle" (UAV) and its historical development are described by Eisenbeiss (2004). Although the definition of UAV has evolved, it has historically been used to describe a remote-controlling flying vehicle without humans on board. UAVs are also referred to as a Remotely Piloted Vehicle (RPV), Remote Controlled Helicopter (RCH), Remotely Operated Aircraft (ROA), or Unmanned Vehicle System (UVS). In terms of applications, UAVs were firstly adopted for military purposes such as reconnaissance, penetration of hostile terrain, and surveillance in remote and high-risk regions (Eck, 2001). Since the 1980s, UAVs started to be applied for photogrammetric purposes. Since then, UAV systems have been widely applied in remote sensing fields, especially for environmental sciences, hazards estimates, agriculture, infrastructure, land use/land cover monitoring, and soil organic carbon estimation (Feng et al., 2021; Nguyen et al., 2022; Shakhatreh et al., 2019; Yao et al., 2019). This development can be attributed to several reasons, such as the advancement of technology in

image processing and the increased availability of low-cost integrated GPS/IMS systems. Images extracted from UAVs have high precision and a very fine spatial resolution, which can reach centimetre precision. UAVs can act as a platform for multiple sensors, including multispectral and hyperspectral images, and light-weight LiDAR sensors (Pajares, 2015; Shahbazi et al., 2014).

Given the above-mentioned advantages, research has shown that UAV technology has been widely used in the field of blue carbon science. For example, Chen and Sasaki (2021) developed a new approach to improve the accuracy of monitoring intertidal and sub-tidal seagrass wetlands in Japan (Chen and Sasaki, 2021). Several attempts have been made to combine field data, multispectral data, and UAV images to accurately estimate tree species (Effiom et al., 2019), carbon stocks (Fernandes et al., 2020), and mangrove AGB (Jones et al., 2020; Otero et al., 2018). They found that UAV data could be the most useful approach to measuring canopy height and biomass for homogeneous and single-height layer forests.

Despite the potential benefits of UAV-based imagery for blue carbon estimates, there are several limitations. For example, Otero et al. (2018) found that there was a considerable difference between ground-based

Table 2
Remote sensing and machine learning techniques for quantifying blue carbon from space.

Blue carbon ecosystem	Method	Sensor	Model performance	Blue carbon range	Study site	Reference
Mangrove	Partial least squares regression (PLSR)	Hyperion	$R^2 = 0.71$	0–46 mg labile C / g soil	Florida, USA	Anne et al. (2014)
	Stochastic Gradient Boosting (SGB)	Landsat-8 OLI	NA	18–159 Mg C ha^{-1} AGC	South Africa	Dube and Mutanga (2015)
	Global dataset and meta-analysis	N/A	NA	569 Mg ha^{-1} AGC 195 Mg ha^{-1} BGC	West Africa	Tang et al. (2015)
	Simple linear regression	ALOS AVNIR-2	0.55–0.69	21.6 Mg C ha^{-1} AGC 5.4 Mg C ha^{-1} BGC	Karimunjawa, Indonesia	Wicaksono et al. (2016)
	Multi-layer perceptron neural networks (MLPNN)	ALOS-2 PALSAR-2	$R^2 = 0.78$	3.2–345.6 Mg C ha^{-1}	Hai Phong city, North Vietnam	Pham et al. (2017)
	Simple linear regression	LiDAR, Landsat-8 OLI	NA	33–57 Mg C ha^{-1} AGC + BGC	Western Australia	Hickey et al. (2018)
	Random forest (RF)	Landsat-5 TM	$R^2 = 0.63$	86–729 Mg C ha^{-1}	Global	Sanderman et al. (2018)
	Random Forests (RF)	UAV	$R^2 = 0.81$	31.7–195.8 Mg C ha^{-1} AGC	Shenzhen Bay, China	Li et al. (2019)
	Global dataset and meta-analysis	N/A	NA	4274–13,767 Mt	Global mangrove	Richards et al. (2020)
	Global dataset and metal-analysis	N/A	NA	237 Mg C ha^{-1}	Global mangrove and salt-marsh	Ouyang and Lee (2020)
	Radial Basis Function (RBF)	Hyperion	$R^2 = 0.87$	27–215 Mg C ha^{-1} AGC	Odisha, India	Anand et al. (2020)
	Simple linear regression	LISS-IV	*NA*	5.2 Mg C ha^{-1}	Kunhimangalam, India	Bindu et al. (2020)
	Simple linear regression	LiDAR and Landsat-5 TM and aerial photographs	$R^2 = 0.90$	40.2 Mg C ha^{-1} AGC	Auckland, New Zealand	Suyadi et al. (2020)
	Simple linear regression	TanDEM-X	*NA*	644–943 Mg C ha^{-1}	Gabon, Africa	Trettin et al. (2021)
	CatBoost (CB) regression	Sentinel-2A and Sentinel-2B	$R^2 = 0.66$	35.1–166.8 Mg C ha^{-1}	North Vietnam	Pham et al. (2021)
	XGBoost regression	Sentinel-2B and Sentinel-1B	$R^2 = 0.76$	2.52 to 123.89 Mg C ha^{-1}	Komodo National Park, Indonesia	Rijal et al. (2023)
Seagrass	Simple Linear Regression	Planet Scope	$R^2 = 0.22$	3,78 Mg C ha^{-1}	Sumatra, Indonesia	Isnaen et al. (2019)
	Simple Linear Regression	Sentinel-2A	NA	19.9 Mg C ha^{-1}	Sulawesi province, Indonesia	Nabil Akbar et al. (2021)
	Allometric equation and LAI	Landsat-5 TM and Landsat-8 OLI	NA	4 Gg BGC	Florida, USA	Lebrasse et al. (2022a)
	In-situ carbon data	Sentinel-2	NA	11.2–40 million Mg C	Kenya, Tanzania, Mozambique and Madagascar	
	CatBoost (CB) regression	Sentinel-1 and Sentinel-2	$R^2 = 0.74$	30–104 Mg C ha^{-1}	Tauranga Harbour, New Zealand	(Ha et al., 2023)
Saltmarsh	Simple linear regression	LiDAR and aerial multispectral photographs	$R^2 = 0.28$–0.47	0.95–2.53 Mg C ha^{-1}	Galveston Island, Texas, USA	Kulawardhana et al. (2014)
	Random Forests (RF)	Landsat-5 TM, Landsat-7 ETM+, Landsat-8 OLI, and Sentinel-1	$R^2 = 0.36$–0.63	1.67–2.67 Mg C ha^{-1}	United States (CONUS)	Byrd et al. (2018)
	Random Forests (RF) and Support Vector machine (SVM)	Worldview-2	$R^2 = 0.66$–0.72	NA	Tomago, Australia	Rasel et al. (2019)
	Ensemble-learning regression	Sentinel-2	$R^2 = 0.59$–0.80	NA	Skinflats and Caerlaverock, Scotland	Ladd et al. (2022)
	Simple linear regression	PlanetScope and ArborCam	$R^2 = 0.26$–0.79	1.32 Mg C ha^{-1}	Jervis Bay, New South Wales, Australia	Warwick-Champion et al. (2022)
	Generative adversarial network (GAN)	Sentinel-2	$R^2 = 0.85$	NA	Shandong Province, China	Chen et al. (2022)
	Random Forests (RF)	UAV-LiDAR	$R^2 = 0.90$	NA	Yangtze River Estuary, China	Tang et al. (2022)

N/A: Not available.

data and the data derived from UAV-system images when tree height was assessed for a heterogeneous species area. To overcome this issue, a combination of simple digital UAV images with hyper-spectral and laser scanning data is a very promising approach. However, the integration of multiple super-high-resolution sensors is costly and still challenging (Brovkina et al., 2017; Luo et al., 2017). With the advancement of remote sensing technology and processing techniques, these central issues are expected to be addressed in the near future.

3. Processing and machine learning approaches for quantifying blue carbon ecosystems

Once data are collected from a passive or active sensor, several data processing and analysis steps can be undertaken. This paper reviews some potential and successful applications of multi-sensor data fusion combined with machine learning techniques and metaheuristic optimization algorithms. Table 2 summarises the current techniques together with their performances for quantifying blue carbon from space using various satellite sensors and regression methods.

3.1. Multivariate regression models

Carbon stock consists of organic carbon in the soil sediments, below-ground biomass (BGB) and above-ground biomass (AGB) of a blue carbon ecosystem. The common method applied for estimating carbon content is a combination of the point-based sampling in the field and further laboratory analysis. Despite a high accuracy of the estimation, this approach leaves the drawbacks of time consuming, intensive field work, and small-scale mapping of the study site. The quantification of blue carbon content using EO data combined with field-based in-situ measurement, therefore is preferred in recent years as a low cost, yet reliable and very scalable to map the spatial distribution of carbon in blue carbon ecosystems.

Field sampling plots can be classified into linear, random, and probability-based grid methods, choosing the suitable method depends on study site accessibility; however, the random and probability grid methods for sampling are recommended (Howard et al., 2014). The literature review shows that a stratified random sampling approach with a size of 100 m^2 has widely used for mangrove and saltmarsh (Chen et al., 2022; Pham et al., 2019b). A sub-plot with 0.5 × 0.5 m is often used to collect biomass of saltmarsh (Chen et al., 2022)whilst a plastic core with 15 cm in diameter and 40 cm in depth is often used for seagrass (Ha et al., 2021a). A number of biophysical parameters of different mangrove species including the tree height (H), diameter at breast height (DBH), canopy diameter (CD) are measured (Pham and Yoshino, 2017) to estimate mangrove above-ground biomass (AGB) using allometric equations (Komiyama et al., 2008). To develop the carbon retrieval models, the relationship between a limited number of field sampling points and the EO data has been established and often results in the form of multivariate regression. For instance, Richards et al. (2020) used the global mangrove dataset (Global Mangrove Watch, https://www.globalmangrovewatch.org/) for quantifying mangrove changes (mangrove loss approximately 800 km^2) at a global scale and implemented the meta-analysis of published dataset, which indicated a temporal loss of mangrove carbon stock (approximately 158 Mt) over time (1996–2016). Global allometric forms, mangrove biomass distribution, and the digital model elevation (DEM) generated from the shuttle radar topography mission (SRTM) are common data sources used to quantify the large scales of mangrove total carbon stocks. For instance, Tang et al. (2015) used the large-scale data of canopy height, to derive biomass using allometric equations in Western Africa. Recently, Tang et al. (2018) proposed an integrated approach, which consisted of GIS-based geospatial data and high-performance parallel computing to estimate mangrove biomass and carbon form the global dataset of mangrove canopy height, biomass, distributional area. However, the uncertainty and accuracy of the estimation are not reported in the studies.

Considering the local and smaller scales, the indirect approach using a conversion factor of carbon content from biomass is widely implemented worldwide. For instance, Hickey et al. (2018) combined LiDAR and Landsat 8 OLI with allometric equations to map mangrove canopy height and estimate the spatial distribution of mangrove AGC stock in north-western Australia while Bindu et al. (2020) adopted the Indian remote sensing (IRS) LISS IV multispectral satellite image to estimate the biomass-derived carbon content from the normalized difference vegetation index (NDVI) data and exponential regression. Similarly, leaf area index (LAI) is a common surrogate used for the estimation of seagrass AGC in different climatic regions. Seagrass LAIs were derived from the Sea-viewing Wide Field-of-View (SeaWiFS) (R^2 ranging from 0.83 to 0.98) (Dierssen et al., 2010), and the Spectroscopic Aerial Mapping System with On-board Navigation (SAMSON) ($R^2 = 0.81$) (Hill et al., 2014), which provided input dataset to quantify the seagrass AGC from various empirical eqs. A small number of in situ LAI plots were used to develop the regression model of LAI from different empirical equations, which were recently developed by Lebrasse et al. (2022a) to deliver the seagrass carbon stock. The study showed promising results in a manner of rationale and cost reduction, however, a magnitude of 20–40% of underestimates was observed (Lebrasse et al., 2022a). Simple linear regression approach has been used to predict the seagrasses AGB, BGB and their soil carbon content (Blume et al., 2023; Traganos et al., 2022). This approach does not provide a precise estimate of blue carbon in saltmarsh ecosystems using PlanetScope and ArborCam ($R^2 = 0.26$) (Warwick-Champion et al., 2022). However, when analysing at the species level, linear regression models are able improve the goodness-of-fits, ranging from 0.62 to 0.79 (Warwick-Champion et al., 2022) (Table 2).

These studies are good examples showcasing the indirect estimation of blue carbon stock from remotely sensed data. The sampling plot size is another important factor that potentially impacts on the accuracy of regression models. This point was validated with a higher accuracy of retrieval model for mangrove AGC estimation using Landsat-8 OLI ($R^2 =$ 0.54–0.61) when compared to the Worldview-2, the ASTER VNIR, the ALOS AVNIR-2 images. Despite a lower spatial resolution, the pixel size of Landsat fitted the plot size at the study site, and therefore derived a more accurate carbon stock map (Wicaksono, 2017). When the inconsistency between the sampling plot and the satellite image pixel size is corrected, the use of higher spatial resolution such as at 10 m of ALOS AVNIR-2 has the potential to improve the indirect retrieval accuracy of AGC and BGC to R^2 of 0.69 and 0.59 using the principal component analysis (PCA) and a carbon conversion factor from mangrove biomass (Wicaksono et al., 2016) (Table 2).

LiDAR is less commonly used for quantifying blue carbon stocks compared to multi-spectral imagery, aerial and hyperspectral images due to their costs and data availability as well as the choice of proposed regression models. For instance, simple linear regression models were developed by Kulawardhana et al. (2014) using multi-spectral aerial photographs and LiDAR data when quantifying saltmarsh carbon stocks in West Galveston Bay on Galveston Island, Texas, USA, showing weak performance ($R^2 = 0.28$–0.47). On the other hand, a good agreement between the mangrove canopy height (derived from the LiDAR image) and the AGC field-derived data ($R^2 = 0.90$) was achieved for a temperate mangrove ecosystem in New Zealand (Suyadi et al., 2020). Other studies have utilised the large number of spectral bands of hyperspectral imagery to derive various soil carbon parameters. For instance, Anne et al. (2014) demonstrate the simple ratio between the spectral reflectance at 0.53 μm and 2.11 μm of Hyperion imagery to accurately derive the soil variables of bulk density ($R^2 = 0.82$), stable carbon ($R^2 = 0.71$), particulate organic matter (POM, $R^2 = 0.67$), and especially the labile carbon with a high accuracy of $R^2 = 0.93$ (Table 2). The common "blue carbon" parameters of soil organic carbon or total carbon were not estimated; however, this study might point the way to further deployment in the mapping of organic carbon from the hyperspectral dataset

and remotely sensed estimates of soil carbon are really only good for the surface soil layer. Despite a potential application, the use of hyperspectral and LiDAR images has drawbacks of small-scale coverage with limited access worldwide and high-cost operation.

3.2. Machine learning models for blue carbon estimation

Machine learning is a non-linear data processing approach, which efficiently handles both classification and regression tasks. Machine learning learns solutions to solve real-world problems at high confidence compared to the traditional approach of parametric regression methods and is easy to combine with various types of space-borne datasets (i.e. multispectral, hyperspectral, SAR images) (Lary et al., 2016; Verrelst et al., 2012). Spectral reflectance and vegetation indices derived from multispectral and/or hyperspectral datasets as well as backscatter coefficients of SAR data have been used as input variables to construct machine learning models. For instance, (Anand et al., 2020) developed a machine learning model using the enhanced vegetation index (EVI) and NDVI derived from Hyperion at 30 m spatial resolution for estimating mangrove AGC at high accuracy ($R^2 = 0.87$). The study extended the potential use of hyper-spectral imagery to detect mangrove species and estimate mangrove AGC. However, the confidence of the estimation depended on the prior classification of mangrove species, biomass estimation, and the number of sampling points for the model validation. Texture information derived from spectral bands has also widely been used as input variables for modelling AGC of mangrove and saltmarsh ecosystem. A texture was adopted for Landsat 8 imagery to extract the mangrove tree structure for the AGC estimation of stem, bark and leaves using the non-parametric ensemble stochastic gradient boosting (SGB) machine learning model (Dube and Mutanga, 2015). Unfortunately, the AGC retrieval accuracy was not reported for the AGC spatial map in this study.

More recently, SAR data such as ALOS-2 PALSAR-2 have been used for estimating mangrove carbon stocks in tropical area using neural networks with promising performance ($R^2 = 0.78$) (Pham et al., 2017). With higher confidence, UAV data were coupled with the Random Forest (RF) algorithm to model the mangrove AGC with an accuracy of $R^2 = 0.81$ using a variety of canopy height, vegetation index (VI), and grey level co-occurrence matrix (GLCM) dataset. Surprisingly, all 88 variables were used to construct the RF regression model, showing the highest accuracy ($R^2 = 0.81$) for mangrove AGC estimation, and the overall accuracy did not improve when using the feature selection (Li et al., 2019) (Table 2).

In an attempt to model saltmarsh AGC stocks for the conterminous United States, Byrd et al. (2018) combined Landsat-TM, ETM+, and OLI+ with Sentinel-1C-band SAR using the RF models. However, despite integrating vegetation indices and dual-polarimetric C-band SAR into the machine learning models, the models' performance was relatively weak, with R^2 values ranging from 0.36 to 0.63 (Table 2). These results suggest that SAR sensors may be less useful for estimating blue carbon in saltmarshes. In a recent study conducted at the Skinflats and Caerlaverock saltmarshes in Scotland, the ensemble-based decision tree models incorporating NDVI derived from Sentinel-2 data and digital terrain model (DTM) were used to estimate SOC stock, showing promising results with R^2 values ranging from 0.59 to 0.80.

More recently, Rijal et al. (2023) used the Extreme Gradient Boosting (XGBoost) algorithm to quantify mangrove AGC at Komodo National Park, Indonesia, while Ha et al. (2023) integrated Sentinel-2 MSI and Sentinel-1 datasets and optimisation algorithms in to the Categorical Boosting (CatBoost) algorithm to map total organic carbon in seagrass beds in New Zealand. These studies suggested that feature selection using metaheuristic optimisation algorithms can improve the model performance of machine learning techniques, archiving an R^2 greater than 0.7 (See Table 2). In summarise, optimisation and feature selection in machine learning techniques are often necessary when dealing with multi-model and multisource remote sensing data.

3.3. Metaheuristic optimisations and feature selection for blue carbon regression

To accurately estimate blue carbon stocks across coastal ecosystems, a combination of different satellite sensors is often required to convey the advantages of specific data, which usually lead to a large number of input features (Rasel et al., 2019). As a result, a feature selection using different statistic and learning techniques is preferred to select the most informative features for carbon stock estimation. This literature review indicates various approaches for this task, in which the metaheuristic optimisation is usually opted due to the capabilities of non-linear learning and precise picking up the best combination of the input bands. Metaheuristic-based feature selection has a wide range applications in different research areas. However, few studies have used this approach to quantify total carbon (TC) or soil organic carbon (SOC) in blue carbon ecosystems. In a typical case study of SOC retrieval in mangrove ecosystem, the Sentinel-2 was combined with the Sentinel-1 and ALOS-2 PALSAR-2, the CatBoost and the Particle Swarm Optimization (PSO) to accurately derive the mangrove SOC at $R^2 = 0.81$ (Le et al., 2021). The PSO provided a manner to reduce the input feature and improve the confidence in SOC estimation from space-borne dataset. Using a similar approach, Pham et al. (2021) developed a novel machine learning model using the Sentinel-2 dataset combined with the CatBoost model, supported by the metaheuristic optimisation genetic algorithm (GA) and achieved a promising result of $R^2 = 0.66$ for estimating mangrove TC stocks. Similarity, Rijal et al. (2023) applied this technique to quantify mangrove AGC at the Komodo National Park in Indonesia and achieved a satisfactory result of $R^2 = 0.76$. In the most recent study reported by Ha et al. (2023), the grey wolf optimization (GWO) was employed to map total organic carbon in seagrass beds in New Zealand with an R^2 of 0.74 (Table 2). These case studies are examples for the application of an open-source satellite dataset and machine learning-based toolset to establish the robust relationship between the field data collection of TC/ SOC with the satellite reflectance/ back-scattering signals. The authors provide novel insights of the multi-spectral and SAR fusion dataset to improve the confident mapping of mangrove TC/ SOC.

3.4. Robust regression using deep learning and transfer learning

Transfer learning is a well-known technique in deep learning architecture that has been widely used for image classification, pattern recognition, and computer vision. Transfer learning aims to propagate knowledge from a source domain to a target domain, showing the potential to calibrate models transferable from one satellite sensor to another (Pires de Lima and Marfurt, 2020). Transfer learning with pre-trained convolutional neural networks (CNNs) has been developed for various remote sensing data analyses, in which the CNN model can learn representative and discriminative features in a hierarchical manner from different remote sensing datasets (Liu et al., 2018). This novel approach is expected to work for regression tasks (Hu et al., 2015; Oquab et al., 2014; Pan and Yang, 2010). Several attempts have been made to quantify SOC using multisource remote sensing data such as hyperspectral combined with the Land Use/Cover Area frame statistical Survey (LUCAS) database at 0–30 cm depth (Liu et al., 2018; Padarian et al., 2019; Yang et al., 2020). Other studies have developed deep neural network regression models to transfer soil reflectance data using hyperspectral imaging (Liu et al., 2017), and have applied deep learning neural networks to map soil properties (Padarian et al., 2019; Yang et al., 2020). These studies show that transfer learning techniques and CNN combined with recurrent Neural Networks (RNN) can suitably predict soil properties using Vis-NIR spectroscopy.

Deep learning has significantly developed at a large number of qualified algorithms with the typical names of CNN, U-Net, residential network (RestNet), RNN, autoencoder (AE), or generative adversarial network (GAN) (Sarker, 2021). Deep learning has been well-developed and widely applied to image segmentation. However, its application

for retrieving biophysical parameters of blue carbon is still in its infancy. Deep learning often requires a large number of samples for model learning and the use of high spatial resolution images, which are significant obstacles preventing its potential utilisation in blue carbon ecosystems. In a recent study, Chen et al. (2022) proposed a GAN with a constrained factor model (GAN-CF) to quantify saltmarsh AGB using hyperspectral imagery and Sentinel-2, achieving a promising result of $R^2 = 0.85$.

3.5. Challenges in blue carbon estimation using machine learning and deep learning

3.5.1. A trade-off between image spatial resolution and available research budget

Commercial satellite imagery provides very high spatial resolution, ranging from 30 cm to less than 10 m, which enables better recognition of habitat patterns and more accurate mapping. It also has the potential to establish closer relationships between field data measurement and carbon stock estimates in blue carbon ecosystems (Qin and Liu, 2022). However, the high cost is the main drawback, especially when considering the large-scale retrieval of carbon stock measures in different ecosystems. Some space-borne commercial satellite imagery (e.g., WorldView, PlanetScope, BlackSky) are expensive when studying on large areas. For instance, WorldView-3 multispectral data with 30 cm spatial resolution may cost US$ 22.5 per km^2 at the georeferenced level without orthorectification. Nevertheless, other space-borne imagery such as Sentinel and Landsat families, offers a free-of-charge plan which is a big advantage for low budget research programmes, though is of a lower spatial resolution (10–30 m) and may leave considerable uncertainty in carbon stock estimation. A coarser spatial resolution may require a more homogeneous and contiguous area to improve the relationship between the reflectance intensity of the satellite image and the field dataset (Wilson et al., 2022), thus enhancing an accurate detection of habitat characteristics. A balance between available budget and the desired spatial resolution must be considered to select the best option of satellite image acquisition whilst accommodating a sufficient budget for further field surveys and laboratory analysis.

3.5.2. Terrestrial and submerged ecosystems

Blue carbon ecosystems include a wide range of terrestrial (mangrove, saltmarsh) and submerged (seagrass) ecosystems. The estimation of AGC is applicable for blue carbon ecosystem stock estimation through the use of allometric equations to derive the stored carbon from the canopy height (Lagomasino et al., 2019; Maeda et al., 2016; Shapiro et al., 2015; Simard et al., 2019; Trettin et al., 2021) and the biomass (Ha et al., 2021b; Pham et al., 2020a; Pham et al., 2020b) or through the LAI data (Hill et al., 2014; Lebrasse et al., 2022a; Lebrasse et al., 2022b). However, BGC and soil carbon retrieval are more challenging due to attenuation by the water column or soil layers, resulting in loss of signal, and reducing the true characteristics of the habitats. Unlike the AGC retrieval, in which the spectral reflectance shows a good correlation to the above-ground carbon content, quantification of BGC or soil carbon require an indirect approach since the signal of the sensor only penetrates into a few millimetres into the sediment of the top soil layer (Le et al., 2021; Pham et al., 2021). In case of seagrass ecosystems, additional impacts of the water column results in the deployment of studies at the low tide condition when seagrass is emerged (Ha et al., 2021b) or couples with a range of water column correction methods (Ha et al., 2020). Despite the success in blue carbon biomass estimation from space, blue carbon stock estimation in both AGC, BGC, and soil carbon is still in infancy with a limited number of observed research papers in this field for mangrove, salt-marsh, and seagrass ecosystems.

3.5.3. Blue carbon field sample and deep learning

Blue carbon ecosystems pose a unique challenge for adopting deep learning methods for carbon quantification from space due to the difficulty of gathering field data. Unlike other image/letter recognition fields, collecting hundreds to thousands of field samples or images of objects is complex and expensive. This makes it challenging to train and validate deep learning models for carbon stock estimation (Politi et al., 2019). To overcome this challenge, future research could develop novel deep learning architectures based on Deep CNN that require less field data for training/validation. Additionally, semi-supervised approaches in deep learning for robust regression should be further developed and tested. These approaches use not only labelled samples but also exploit unlabelled samples. Co-training algorithms for semi-supervised regression have also been developed to make use of unlabelled samples, providing more accuracy (Hong et al., 2020). Alternatively, human-in-the-loop techniques such as active learning could be applied to guide the manual labelling process, aided by UAV for ground truth data annotation for deep learning models. Consideration should be given to the relative costs, benefits, and trade-offs of supervised learning for blue carbon estimation (Kellenberger et al., 2019; Kellenberger et al., 2020).

4. Remote sensing and machine learning techniques for quantifying blue carbon dynamics

Monitoring blue carbon stocks and their changes from space often requires time-series EO datasets. Multi-temporal EO data offers useful information on the spatial distribution and extent, temporal changes of the mangroves, seagrasses, and tidal marshes (Lebrasse et al., 2022a; Pham et al., 2019b). However, precise and robust estimates of blue carbon changes are challenging tasks due to difficulties and uncertainties for the change detection approaches of blue carbon dynamics (Farzanmanesh et al., 2021). This section provides information on up-to-date remote sensing techniques and highlights the effective monitoring methods using machine learning techniques for quantifying blue carbon changes.

4.1. Remote sensing data for quantifying blue carbon dynamics

Several attempts have been made in quantifying blue carbon dynamics using multi-temporal EO data. Landsat time-series datasets have widely used to monitor blue carbon changes whereas Sentinel-1 and Sentinel-2 data were recently applied for quantifying mangrove and saltmarsh (Table 3). Canopy height models are the most common approaches to deliver carbon stocks in mangrove ecosystems (Lagomasino et al., 2019; Maeda et al., 2016; Shapiro et al., 2015; Simard et al., 2019; Trettin et al., 2021). Previous studies employed SRTM and Ice, Cloud, and land Elevation Satellite (ICESat) Geoscience Laser Altimeter System (GLAS) datasets to derive mangrove canopy height and then mangrove biomass and total carbon stocks were estimated using height-based approach with a conversion factor to transform mangrove height into belowground carbon and soil carbon stocks. For instance, Shapiro et al. (2015) used SRTM data calibrated with ICE Sat/GLAS data to derive mangrove canopy height and detect mangrove carbon dynamics. Recently, Lagomasino et al. (2019) employed Sentinel-1C-band SAR and TerraSAR-X together with SRTM to estimate mangrove carbon stocks change between 2000 and 2016. However, the performance and uncertainties of models were not reported. More recently, Lebrasse et al. (2022b) reported on the extent of seagrass carbon in Florida, USA using time-series Landsat dataset, while Blume et al. (2023) used multi-temporal Sentinel-2 data within the Google Earth Engine cloud computing platform to assess the national extent, blue carbon stock, and sequestration rate of seagrass ecosystems across the shallow waters of the Bahamas (Table 3).

Simple-linear and multi-linear regression models showed weak performances ($R^2 = 0.35$–0.47) for estimating mangrove blue carbon and assessing their carbon stocks dynamics (Bolivar et al., 2018) whilst a linear conversion from LAI was applied to derive the variation of seagrass carbon stock Lebrasse et al. (2022b). On the other hand, machine learning techniques, particularly ensemble-based decision tree family

Table 3
Methods for monitoring blue carbon dynamics using multi-temporal remotely sensed data.

Blue carbon ecosystem	Method	Sensor	Model performance	Blue carbon changes period	Study site	Reference
Mangrove	Canopy Height model	Landsat-7 ETM+ and Landsat-8 OLI plus SRTM and ICESat/GLAS	*N/A*	1994–2013	Zambezi Delta, Mozambique	Shapiro et al. (2015)
	Canopy Height model	RapidEye, Landsat and airborne LiDAR	*N/A*	1989–2012	South Sumatra, Indonesia	Maeda et al. (2016)
	Random Forest (RF)	SPOT-4 and SPOT-5	$R^2 = 0.73$	2000–2011	Can Gio, Vietnam	Pham and Brabyn (2017)
	ANOVA	Landsat-7 ETM+ Landsat-8 OLI	*N/A*	2000–2014	Southwest Madagascar	Benson et al. (2017)
	Random Forest	Landsat-5 TM Landsat-7 ETM+ Landsat-8 OLI	*N/A*	1990–2017	Malaysia	Omar et al. (2018)
	Multi-linear regression model	MODIS	$R^2 = 0.35–0.47$	2011–2013	Colombia	Bolivar et al. (2018)
	Linear latitudinal model	Landsat-5 TM, Landsat-8 OLI	*N/A*	2000–2012	Global	Hamilton and Friess (2018)
	Canopy height model	SRTM, ICESat/GLAS	*N/A*	2003–2009	Global	Simard et al. (2019)
	Canopy Height model	Landsat-8 OLI Sential-1C SRTM TerraSAR-X	*N/A*	2000–2016	Asia and Africa	Lagomasino et al. (2019)
Seagrass	Conversion from LAI	Landsat-5 TM and Landsat-8 OLI	N/A	1990–2020	Florida, USA	Lebrasse et al. (2022b)
	Conversion from areal carbon stock range	Sentinel-2A	N/A	2017–2021	Bahamas	Blume et al. (2023)
Mangrove and saltmarsh	Random Forest (RF)	Landsat-8 OLI and Sentinel-2A	$R^2 = 0.87$	2015–2019	Indonesia	Sejati et al. (2020)

N/A: Not available.

such as the RF, the XGBoost algorithms have recently employed with a promising results, with an R^2 ranging from 0.73 to 0.87 in retrieving blue carbon in mangrove and saltmarsh ecosystems (Pham and Brabyn, 2017; Sejati et al., 2020) (Table 3).

4.2. Challenges in quantifying blue carbon from space

4.2.1. Atmospheric and geometric effects on blue carbon retrievals

Multispectral and hyperspectral data often require atmospheric correction to minimize atmospheric conditions such as sunglint, aerosols, and water vapour content, particularly in forested areas (Lausch et al., 2020; Nguyen et al., 2015; Zhu et al., 2015), and over coastal wetlands environments (Pereira-Sandoval et al., 2019; Warren et al., 2019). Sunglint can have a significant impact on atmospheric correction in remote sensing, particularly in blue carbon ecosystems. Sunglint refers to the specular reflection of sunlight on the water surface, which can create a bright spot on an image of the water surface. When performing atmospheric correction, sunglint may cause inaccuracies in the estimation of the water-leaving radiance, which is the radiance of light leaving the water surface. This is because the sunglint may cause an overestimation of the radiance in that area. A number of algorithms can be used to estimate the effect of sunglint on the radiance measurements and correct for it in the atmospheric correction process (Harmel et al., 2018). Different methods for atmospheric correction (AC) have been proposed and developed for certain areas to overcome the limitations such as inland waters in mangrove and saltmarsh ecosystems or turbid coastal water in seagrass ecosystems (Lam-Dao et al., 2011; López-Serrano et al., 2016; Maciel and Pedocchi, 2022; Pons et al., 2014; Xu et al., 2012). For instance, Ilori et al. (2019) compared performance of the four AC algorithms such as the Atmospheric and Radiometric Correction of Satellite Imagery (ARCSI), the Atmospheric Correction for OLI 'lite' (ACOLITE), the Landsat 8 Surface Reflectance (LSR) Climate Data Record (Landsat CDR), and the Sea-Viewing Wide Field-of-View Sensor (SeaWiFS) Data Analysis System (SeaDAS) for Landsat-8 OLI and concluded that the SeaDAS and the ACOLITE models, which are open-source software developed using Python scripts, performed better. Pereira-Sandoval et al. (2019) evaluated the five different AC algorithms over inland waters for Sentinel-2 MSI and figured out that the Polynomial-based (POLYMER) and the Case 2 Regional Coast Colour (C2RCC) algorithms showed the best statistics. Several well-known techniques for AC include the Dark Object Subtraction (DOS), the Second Simulation of Satellite Signal in the Solar Spectrum models (6S), the fast line-of-sight atmospheric analysis of the spectral hypercubes (FLAASH) available in ENVI commercial software, the Atmospheric CORection (ATCOR), and the Image correction for atmospheric effects (iCOR), the ACOLITE for optical sensors i.e. Landsat-5 TM, Landsat-7 ETM+, Landsat-8 OLI, SPOT-5, and WorldView-2 (Balthazar et al., 2012; López-Serrano et al., 2016; Nguyen et al., 2015; Pancorbo et al., 2021) and the Sen2Cor available free-of-charge in the Sentionel-2 toolbox developed using Java scripts for Sentinel MSI data (Martins et al., 2017; Pereira-Sandoval et al., 2019).

For SAR data, speckling or 'salt and pepper' noise is a common issue that affects the model performances of AGC, BGC and SOC retrievals. Despeckling or denoising of SAR imagery by employing a local filter such as the Lee, the enhanced Lee, the Frost, the Wedge, and the block matching 3D filters can retain image features and reduce noise (Painam and Manikandan, 2021). However, the local filtering techniques may cause blurring on filtered images that influence the goodness-of-fits of regression model for retrieving blue carbon estimates. Nonlocal filters for removing speckle of SAR images (Baier et al., 2017; Qiu et al., 2004; Zhong et al., 2011; Zhu et al., 2013), should be computed cautiously to tackle the drawbacks of noise before a regression modelling. Furthermore, surface roughness is an important factor to consider while working with SAR data, as it can have a significant impact on the quality and accuracy of the resulting images. When a surface is rough, electromagnetic waves tend to scatter in multiple directions, leading to a more diffuse backscattered signal. This can make it challenging to interpret the SAR data precisely. Additionally, rough surfaces can create shadows on the ground, which may cause areas of reduced SAR backscatter, making it difficult to differentiate between areas of high and low backscatter in the SAR image (Painam and Manikandan, 2021; Touzi et al., 2022). To overcome the limitations associated with the use of SAR

data for quantifying blue carbon from space, it is necessary to perform calibration and validation techniques for polarimetric SAR beforehand.

4.2.2. Spectral and spatial resolutions on blue carbon estimation

Blue carbon estimates are limited by the different spectral, spatial, and radiometric resolutions of EO datasets. Landsat mission, which consisted of Landsat-5 TM, Landsat-7 ETM+, Landsat-8 OLI, and Landsat-9 OLI-2 sensors, offers medium spatial resolution at 30 m while Sentinel-2A and —2B sensors provide better spatial resolution at 10 m (Drusch et al., 2012; Masek et al., 2020). Landsat time-series datasets are the most common free-of-charge EO data source for quantifying blue carbon dynamics in the current literature. The most recent Landsat-9 OLI-2 has continued offering higher radiometric resolution with 14-bits quantization, which were increased from 12-bits of Landsat-8 and 8-bits of Landsat-7 and Landsat-5. Additionally, Landsat-9 sensor provides only 9 spectral bands whereas Sentinel MSI offers better spatial and spectral resolutions with 13 spectral bands, of which the three Red-edge bands with central wavelengths ranging from 704 to 783 nm play an important role for blue carbon retrievals. It is likely due to the strong absorption features of different soil types at the NIR-SWIR spectra caused by bending and stretching of the O—H and the N—H groups, and the C—H bonds (Gholizadeh and Kopačková, 2019). Recently, Le et al. (2021) and Pham et al. (2021) showed that the Red-edge bands and the Inverted red-edge chlorophyll index (IRECl) and the Modified chlorophyll absorption in reflectance index (MCARI) derived from the Sentinel-2 imagery are the most sensitive to mangrove SOC estimates. Similar observations were reported by Ha et al. (2021b) when modelling seagrass AGC in New Zealand estuary, showing the highest correlations between seagrass AGC and the IRECl and the MCARI indices. Hyperspectral imaging has the potential to address some of these drawbacks, thanks to its ability to capture a wider range of spectral bands compared to other imaging techniques (Lu, 2006). However, it is important to note that hyperspectral imaging is mostly obtained from airborne sensors, which have limited capabilities for capturing data in certain blue carbon ecosystems.

5. Data fusion and multimodal EO data for blue carbon retrievals

5.1. Multisource remote sensing data fusion

As multispectral, hyperspectral, and SAR sensors have different attributes in reflecting structures in blue carbon ecosystems, an integration of multimodal EO data or data fusion can enhance the capability of a regression model for blue carbon estimation. For instance, hyperspectral data are often available only at coarser spatial resolution than multispectral data, thus fusing them with pan-sharpening techniques may improve its spatial resolution. Using multi-sensor data fusion can offer alternative approaches to improving estimates of blue carbon using machine learning techniques, as incorporating data from multiple sensors or sources with different resolutions means the algorithm can learn from a wider range of features.

New advances in the space industry and computer science have led to the availability of large multi-modality datasets, which combine different remote sensing data types to extract more information. Single modality datasets have limitations due to the disadvantages of each sensor, which can result in lower accuracy for objects with similar spectral characteristics or located below the surface (Ha et al., 2021b; Le et al., 2021; Stovall et al., 2021). Combining multimodal images with advanced machine learning and metaheuristic optimization can improve regression accuracy for quantifying blue carbon (Table 4).

Multisource data fusion combined with advanced machine learning and metaheuristic optimisation algorithms are expected to resolve the limits of a single remote sensing sensor and/or simple multi-linear regression for quantifying blue carbon from space. Recently, multi-modal and multisensor EO datasets have been successfully used for improving estimates of mangrove blue carbon in Vietnam (Le et al., 2021) and in Indonesia (Rijal et al., 2023). Optimisation for feature selection has been widely applied to quantify blue carbon in mangrove and seagrass ecosystems with promising results, with R^2 values greater than 0.70 (Table 4). Le et al. (2021) developed an automated framework (Fig. 3) using Sentinel 2 MSI, Sentinel-1C-band, and ALOS-2 PALSAR-2 to predict mangrove SOC in Vietnam. They used the CatBoost decision tree technique and particle swamp intelligence to optimize features and achieved a promising result ($R^2 = 0.81$) for quantifying mangrove SOC in the tropics. The framework was developed using open-source Python code.

For blue carbon ecosystems, SAR, optical, and LiDAR data are available and there is great potential for further fusion to take advantage of this imagery. The SAR sensor signal is capable of penetrating through cloud and acquiring imagery in both day-time and night-time, and in different weather conditions, a property extremely useful for monitoring the carbon pools since blue carbon ecosystems are widely distributed in humid tropical and sub-tropical regions (Pham et al., 2019b). Despite a limited capability of penetration, the multi-spectral sensor provides valuable spectral information on the observed objects and therefore, support the extraction of designated parameters at surface and below-surface areas. On the other hand, the LiDAR sensor is not affected by weather conditions and has the ability to capture images with greater depth. This improves the spatial resolution, allowing retrieval models to estimate biophysical characteristics more accurately (Malerba et al., 2023). The fusion of the multi-modality dataset using the SAR, multi-spectral and LiDAR sensors may represent a breakthrough in carbon budget estimation and monitoring worldwide.

To fuse data from a variety of multi-modalities, the user can either combine different inputs or translate the data in one and apply to another data types (i.e. SAR, LiDAR, multispectral data). The first approach using shallow models for multi-modality learning (MML) (Hong et al., 2021) is a common practice as different observations for forest biomass, canopy height estimation in the literature by using morphology-based fusion, subspace learning or simply integrating input bands from various sensors (Li et al., 2020), which supports to extract further information of multi-sensor and helps the algorithms to learn better the relationship between the target variable such as AGB and the multispectral bands. The latter approach using deep learning techniques for different modality learning (DML) or cross-modality learning (CML)

Table 4
Data fusion, advanced machine learning techniques and metaheuristic optimisation used for quantifying blue carbon from space.

Blue carbon ecosystem	Method	Fused data	Model performance	Blue carbon range	Study site	Reference
Mangrove	CatBoost and Particle Swarm Optimisation (PSO)	Sentinel-2, Sentinel-1 and ALOS-2 PALSAR-2	$R^2 = 0.81$	44.74 to 91.92 Mg C ha^{-1}	Red River Delta, Vietnam	Le et al. (2021)
	XGBoost and Genetic Algorithm (GA)	Sentinel-2 and Sentinel-1	$R^2 = 0.76$	2.52 to 123.89 Mg C ha^{-1}	Komodo National Park, Indonesia	Rijal et al. (2023)
Seagrass meadow	XGBoost and PSO	Sentinel-2 and Sentinel-1	$R^2 = 0.75$	15 to 201 g DW m^{-2}	New Zealand estuary	Ha et al. (2021b)
	CatBoost and Grey Wolf Optimisation(GWO)	Sentinel-2 and Sentinel-1	$R^2 = 0.74$	30 to 60 Mg C ha^{-1}	New Zealand estuary	Ha et al. (2023)

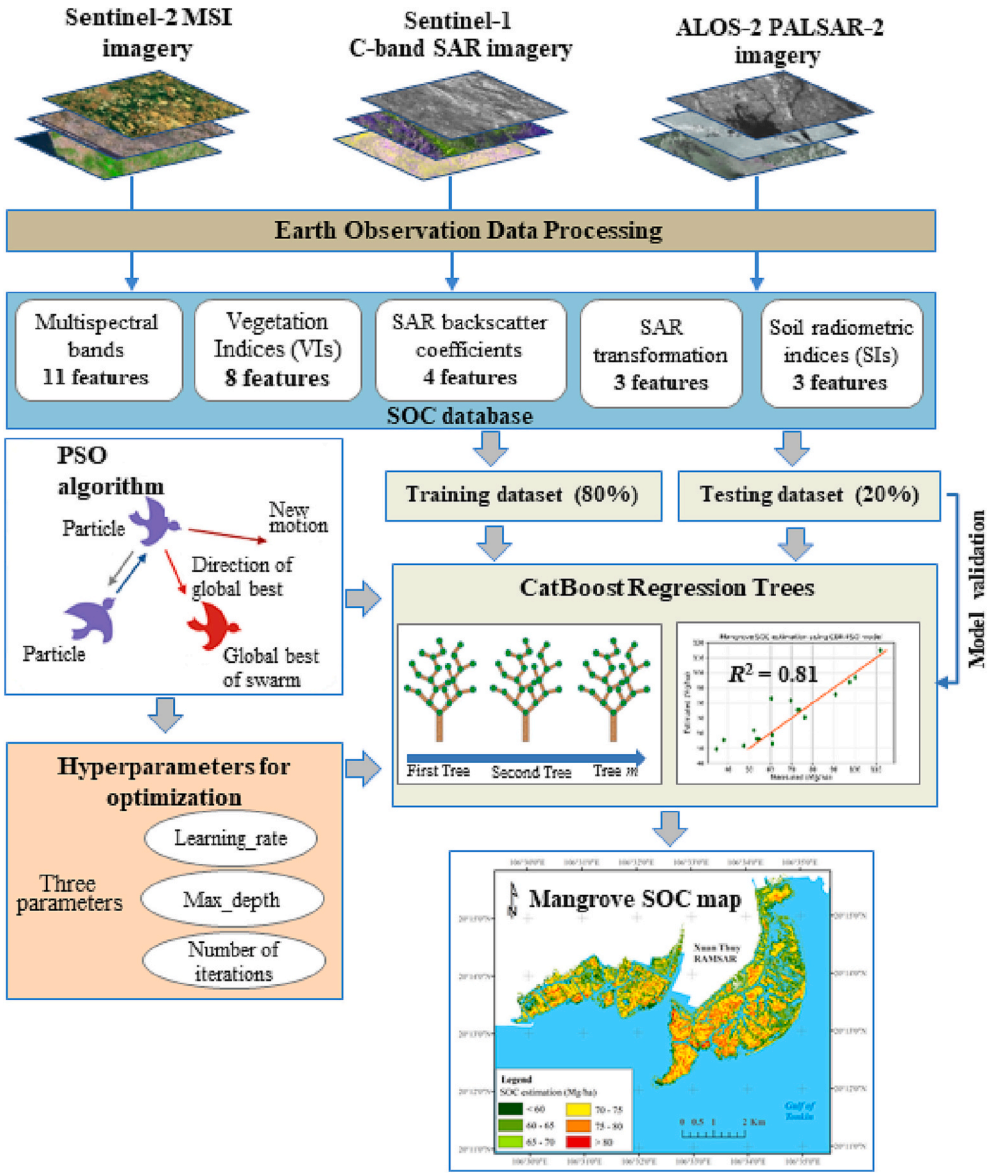

Fig. 3. Framework for quantifying mangrove SOC from multisource remote sensing data combined with advanced machine learning techniques Source: Adopted from Le et al. (2021).

(Hong et al., 2021; Hughes et al., 2020), deals with the more challenging task of the algorithm learning knowledge from one data type (SAR data) and transferring this to another data type (multi-spectral data) to obtain the desired target. Stacking layers of different input data types is easier as the user only need to collect the inputs and let the algorithm handle the entire learning process.

5.2. Challenges in data fusion and multimodal modes for quantifying blue carbon

The DML method aims to extract information from one modality, such as SAR data, and use it to retrieve the desired target in another modality, such as optical data. However, the reference information used for the former is only available in one modality and may not be present in the other (Xia et al., 2022). The use of deep neural network architectures, along with a self-training module, has shown promising results for analysing multi-modal datasets. However, it can be more challenging in practice as the user needs to learn features from one modality (e.g., SAR data) and design a framework to transfer that knowledge to other modalities, such as multi-spectral or UAV data. This allows the machine learning and deep learning algorithms to learn new features and derive accurate and robust results (Zheng et al., 2021). DML and MML approaches, combined with VHR imagery from multi-spectral and SAR sensors, have the potential to improve the accuracy of carbon stock retrieval in blue carbon ecosystems. However, these models need to be made simpler to implement, consume less training data, and deal with the sparser spatial resolution of common satellite sensors. A strategy of semi-supervised, weak supervision, or self-supervision learning would be more adaptive and could help to address the current challenges for carbon content estimation. In addition to deep models, shallow models should also be further developed to provide a more rational solution not only for mangrove forests and saltmarshes but also for underwater seagrass meadows.

5.3. Recommendations for quantifying blue carbon from space

Several future directions exist for quantifying blue carbon in mangrove, seagrass, and saltmarsh ecosystems and monitoring their carbon dynamics including the choice of EO datasets, the use of cloud-based processing platform and the application of ML and DL

approaches for an accurate quantification of blue carbon at a large scale from space (Table 5). We recommend the combination of multispectral and SAR data for quantifying mangrove and saltmarsh ecosystems whereas multisource optical sensors would be useful for the estimation of seagrass blue carbon. In the diverse environment of blue carbon ecosystems, a global approach for carbon stock estimation in different climatic regions is not feasible and therefore, EO data fusion in MML, DML, and CML forms is suggested to leverage the advances of the EO sensors, which support the variety of input datasets to extract different local characteristics for carbon quantification. In addition, advanced machine learning techniques and novel deep learning architectures using high performance computing (HPC) environment developed in Python scripts allow for the rapid and repeatable assessment of the current state and changes of blue carbon ecosystems. Metaheuristic optimization provides a workflow to reduce the dimension of the multi-modal dataset, lessening computation cost while providing the potential for improving the accuracy of the retrieval model.

6. Fast computing for future blue carbon estimates from space

The high-dimensional remote sensing images of multispectral, hyperspectral, SAR, LiDAR, and UAV datasets, particularly very high spatial resolution often requires advanced processing techniques and HPC for accelerating multisource EO data-related computations to quantify blue carbon (Keogh and Mueen, 2010). Generally, software for remote sensing analysis has been run on a single computer with a single central processing unit (CPU) in solving classification or regressions tasks. Each task is executed one by one, a highly time-consuming process when dealing with a large volumes of EO data (Christophe et al., 2011). On the other hand, parallel computing allows multiple use of computing resources to be run on multiple CPUs, which are considered as Graphic processing units (GPU) (Christophe et al., 2011; Li et al., 2018). Recently, the GPU has widely used in remote sensing image analysis to minimize task idle time.

Recent advances of fast computing and a number of novel techniques have been developed to accelerate multisource remote sensing data. In this section, we summarise some of available useful tools, which may be effective for monitoring blue carbon ecosystems using the adopted platform for fast computing.

Table 5
Recommendation for quantifying blue carbon ecosystems and monitoring their carbon changes from space.

Task	EO data	Recommendation
Mangrove carbon	Tan DEM-X, TerraSAR-X ALOS-2 PALSAR-2 Air-borne LiDAR Sentinel-2 and Sentinel-1	Canopy height models Machine learning (XGBoost, CatBoost models) and Deep learning
	Tan DEM-X, TerraSAR-X ALOS-2 PALSAR-2 Air-borne LiDAR Sentinel-2 and Sentinel-1	Canopy height model XGBoost CatBoost
Saltmarsh carbon	Tan DEM-X, TerraSAR-X ALOS-2 PALSAR-2 Sentinel-2 and Sentinel-1	XGBoost, CatBoost models and metaheuristics optimisation and Deep learning
Seagrass meadow carbon	Sentinel-2 Planet Scope ALOS AVNIR-2 and ALOS-3 MS	XGBoost, CatBoost models and metaheuristics optimisation and Deep learning
Monitoring mangrove carbon dynamics	Landsat time-series and Sentinel-2A and 2B	Data fusion, Machine learning on GEE
Monitoring saltmarsh carbon dynamics	Landsat time-series and Sentinel −1 and Sentinel - 2	Data fusion, Machine learning on GEE
Monitoring seagrass meadows carbon dynamics	Landsat time-series and Sentinel-2A and 2B	Data fusion, Machine Learning on GEE

6.1. Hardware accelerators

The GPU is one of the most common HPC architectures and has shown excellent performance when dealing with high dimensionality issue of multisource remote sensing data (Nickolls and Dally, 2010). The compute unified device architecture (CUDA) is a novel technology of general purpose computing on the GPU, that has recently applied in image processing domain as it offers massive speed and parallel computation (Bernabe et al., 2013; Yang et al., 2008). This has motivated the potential use of GPUs for processing big EO datasets for a large scale monitoring blue carbon dynamics.

6.2. Cloud computing (GEE, AWS)

Researchers have recently been using cloud computing platforms, such as Google Earth Engine (GEE), and Amazon Web Services (AWS) to map mangrove dynamics using time-series Landsat and/or Sentinel-2 MSI datasets (Chen et al., 2017; Ghorbanian et al., 2021; Hu et al., 2020; Wang et al., 2020; Yancho et al., 2020) and seagrass meadows (Li et al., 2022; Traganos et al., 2018) as well as saltmarshes (Byrd et al., 2018). Cloud computing offers advanced capabilities for real-time implementation of remotely sensed data classification (Sánchez et al., 2015; Torti et al., 2016). The GEE cloud computing platform has the capability to automatically monitor blue carbon systems by utilising time-series multispectral datasets such as Landsat and Sentinel-2 missions, as well as SAR datasets such as Sentinel-1C-band (Fig. 4). For instance, Vu et al. (2022) used multi-temporal Landsat time-series data on the GEE to monitor mangrove dynamics in Vietnam for 32 years. Subsequently, the mangrove database can be used to monitor mangrove blue carbon changes when combined with temporal field data and the geospatial system is thereby able to automatically update mangrove carbon map for the Vietnam coastline. In a study conducted by Blume et al. (2023), the RF algorithm was applied to map seagrass using time-series Sentinel-2A imagery on the GEE and quantify seagrass carbon stocks in the Bahamas using region-specific in-situ carbon data such as Tier 1 and Tier 2 assessments following by Howard et al. (2014). Near-real time monitoring using GEE also offers potential applications for decision support of blue carbon dynamics in dealing with climate change impacts. Additionally, the potential use of cloud computing for big EO data can be considered an ideal solution due to the evolution of machine learning and deep learning techniques developed in other domains such as medical imaging, computer vision, and pattern recognition. Particularly, the applications of GPUs has been extended worldwide thanks to the increasing development of well-known deep learning frameworks such as TensorFlow, PyTorch, Keras, Spark, which have their applications in satellite image analysis (Kumar et al., 2021; Neupane et al., 2021). However, to date there are very few applications for the use of cloud computing for the implementation of multisource EO data for automatically quantifying blue carbon ecosystems. This is likely due to the lack of open repositories of remotely sensed images available for public utilisation. This is expected to change in the near future since a large number of distributed repositories of multispectral, hyperspectral, SAR, UAVs, and LiDAR data for image classification and regressions have recently released for public use and available to the remote sensing community.

6.3. Challenges in fast computing

The greatest difficulty associated with the consolidation of fast computing techniques for satellite image analysis, particularly in the context of real-time monitoring is the cost for purchasing a HPC and its

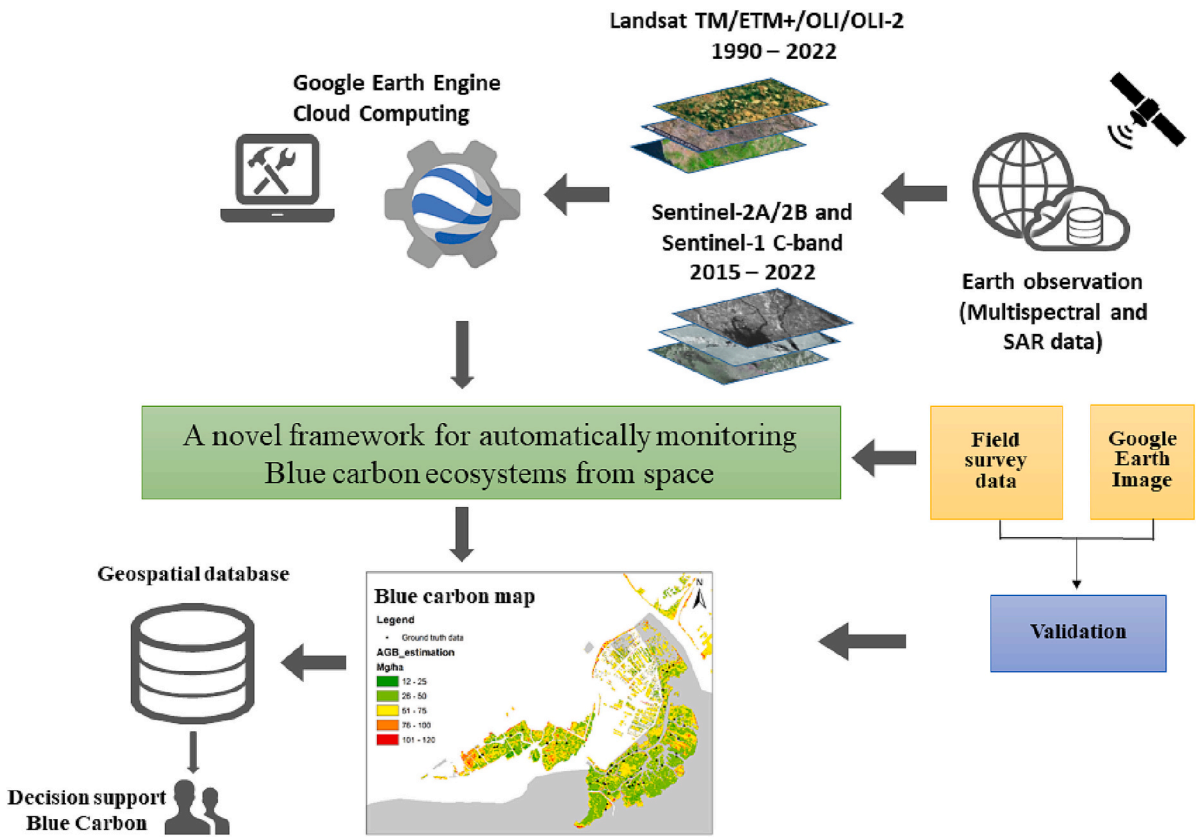

Fig. 4. Google Earth Engine Cloud computing for decision support for quantifying blue carbon ecosystems.

high energy consumption required for running and maintaining HPC architectures (Ghamisi et al., 2017). The electrical demand required by devices such as GPUs is extremely high for their incorporation into satellite platforms. Additionally, these platforms have radiation tolerance issues that require well-trained computer science engineer to operate. Importantly, selecting the suitable machine learning and/or deep learning algorithms for rapidly processing multisource EO data can be challenging as different algorithms may produce better results but may also require more computational resources compared to simpler algorithms such as the RF and the SVM algorithms (Ghamisi et al., 2017). Further developments in hardware instruments for on-board operation are necessary for efficiently processing EO data for quantifying blue carbon ecosystem in the near future.

7. Conclusions

Blue carbon ecosystems play an important role in supporting coastal habitats, through provision of numerous ecosystem services including biodiversity and fisheries enhancement, and acting as a sink of carbon dioxide and thereby reducing the severity of global warming. They have received increasing attention over the past decade and considered as emerging nature-based solutions in dealing with climate change impacts. This has resulted in a rapid increase in the number of research studies quantifying AGC, BGC and soil carbon stocks and monitoring blue carbon dynamics using various EO datasets, ranging from medium to high spatial resolution of hyperspectral imaging, multispectral SAR data, LiDAR, and UAV systems.

Our review shows that the most commonly used sensors for assessing blue carbon changes have been from the Landsat family, but recent studies are incorporating other sensors such as Sentinel-2 MSI and Sentinel-1C-band SAR. Canopy height models derived from SAR and LiDAR datasets are frequently used for estimating mangrove biomass and total carbon stocks globally, but SAR sensors may not be as useful for submerged seagrass and aquatic environments, while LiDAR may not be suitable for submerged plant canopy from the bottom. There is potential for using UAVs to aid in ground truth data annotation for developing deep learning architectures.

Cloud computing platforms, such as GEE, offer alternative approaches for quantifying blue carbon from space and should be further explored in future studies. Incorporating species-level classification data for blue carbon retrievals using machine learning approaches can improve the effectiveness and robustness of regression models. Data fusion, combined with advanced machine learning techniques, such as ensemble-based decision tree algorithms and metaheuristic optimisations, has proven to be useful for estimating blue carbon stocks and monitoring their carbon change. Machine learning approaches are likely to become more attractive in the remote sensing domain, particularly active learning and semi-supervised learning, which can be useful in dealing with limited field data for quantifying blue carbon ecosystems. Recent developments in deep learning also show promising applications for large-scale estimates. Continued advancements in remote sensing and artificial intelligence (AI) technologies as well as increased collaboration between researchers, policymakers, and stakeholders will be necessary to accurately quantify the global carbon sequestration potential of blue carbon ecosystems and to invest in blue carbon offset projects in the future.

Declaration of Competing Interest

The authors declare that they have no known competing financial interests or personal relationships that could have appeared to influence the work reported in this paper.

Data availability

No data was used for the research described in the article.

Acknowledgements

This research was supported by Macquarie University under the Macquarie University Research Fellowship awarded to Tien Dat Pham (Grant No. MQRF0001124-2021).

References

Anand, A., Pandey, P.C., Petropoulos, G.P., Pavlides, A., Srivastava, P.K., Sharma, J.K., Malhi, R.K.M., 2020. Use of hyperion for mangrove forest carbon stock assessment in Bhitarkanika Forest Reserve: a contribution towards blue carbon initiative. Remote Sens. 12 (4), 597.

Anne, N.J.P., Abd-Elrahman, A.H., Lewis, D.B., Hewitt, N.A., 2014. Modeling soil parameters using hyperspectral image reflectance in subtropical coastal wetlands. Int. J. Appl. Earth Obs. Geoinf. 33 (1), 47–56.

Apostolopoulos, D., Nikolakopoulos, K., 2021. A review and meta-analysis of remote sensing data, GIS methods, materials and indices used for monitoring the coastline evolution over the last twenty years. Eur.J.Remote Sens. 54 (1), 240–265.

Baier, G., Rossi, C., Lachaise, M., Zhu, X.X., Bamler, R., 2017. In: Nonlocal InSAR filtering for high resolution DEM generation from TanDEM-X interferograms, 2017 IEEE International Geoscience and Remote Sensing Symposium (IGARSS), pp. 103–106.

Balthazar, V., Vanacker, V., Lambin, E.F., 2012. Evaluation and parameterization of ATCOR3 topographic correction method for forest cover mapping in mountain areas. Int. J. Appl. Earth Obs. Geoinf. 18, 436–450.

Bamler, R., 2000. Principles of synthetic aperture radar. Surv. Geophys. 21 (2–3), 147–157.

Benson, L., Glass, L., Jones, T.G., Ravaoarinorotsihoarana, L., Rakotomahazo, C., 2017. Mangrove carbon stocks and ecosystem cover dynamics in Southwest Madagascar and the implications for local management. Forests 8 (6), 190.

Bernabe, S., Lopez, S., Plaza, A., Sarmiento, R., 2013. GPU implementation of an automatic target detection and classification algorithm for hyperspectral image analysis. IEEE Geosci. Remote Sens. Lett. 10 (2), 221–225.

Beyan, C., Browman, H.I., 2020. Setting the stage for the machine intelligence era in marine science. ICES J. Mar. Sci. 77 (4), 1267–1273.

Bindu, G., Rajan, P., Jishnu, E.S., Ajith Joseph, K., 2020. Carbon stock assessment of mangroves using remote sensing and geographic information system. Egypt. J. Remote Sens. Space Sci. 23 (1), 1–9.

Blume, A., Pertiwi, A.P., Lee, C.B., Traganos, D., 2023. Bahamian seagrass extent and blue carbon accounting using Earth observation. Front. MarineSci. 10.

Bolivar, J.M., Gutierrez-Velez, V.H., Sierra, C.A., 2018. Carbon stocks in aboveground biomass for colombian mangroves with associated uncertainties. Reg. Stud. Mar. Sci. 18, 145–155.

Brovkina, O., Novotny, J., Cienciala, E., Zemek, F., Russ, R., 2017. Mapping forest aboveground biomass using airborne hyperspectral and LiDAR data in the mountainous conditions of Central Europe. Ecol. Eng. 100, 219–230.

Bunting, P., Rosenqvist, A., Hilarides, L., Lucas, R.M., Thomas, N., 2022. Global mangrove watch: updated 2010 Mangrove Forest Extent (v2.5). Remote Sens. 14 (4), 1034.

Byrd, K.B., Ballanti, L., Thomas, N., Nguyen, D., Holmquist, J.R., Simard, M., Windham-Myers, L., 2018. A remote sensing-based model of tidal marsh aboveground carbon stocks for the conterminous United States. ISPRS J. Photogramm. Remote Sens. 139, 255–271.

Campbell, A.D., Fatoyinbo, T., Charles, S.P., Bourgeau-Chavez, L.L., Goes, J., Gomes, H., Halabisky, M., Holmquist, J., Lohrenz, S., Mitchell, C., Moskal, L.M., Poulter, B., Qiu, H., Sousa, C.H.R.D., Sayers, M., Simard, M., Stewart, A.J., Singh, D., Trettin, C., Wu, J., Zhang, X., Lagomasino, D., 2022. A review of carbon monitoring in wet carbon systems using remote sensing. Environ.Res.Lett. 17 (2), 025009-025009.

Cao, J., Liu, K., Zhuo, L., Liu, L., Zhu, Y., Peng, L., 2021. Combining UAV-based hyperspectral and LiDAR data for mangrove species classification using the rotation forest algorithm. Int. J. Appl. Earth Obs. Geoinf. 102, 102414.

Chen, B., Xiao, X., Li, X., Pan, L., Doughty, R., Ma, J., Dong, J., Qin, Y., Zhao, B., Wu, Z., Sun, R., Lan, G., Xie, G., Clinton, N., Giri, C., 2017. A mangrove forest map of China in 2015: Analysis of time series Landsat 7/8 and Sentinel-1A imagery in Google Earth Engine cloud computing platform. ISPRS J. Photogramm. Remote Sens. 131, 104–120.

Chen, C., Ma, Y., Ren, G., Wang, J., 2022. Aboveground biomass of salt-marsh vegetation in coastal wetlands: sample expansion of in situ hyperspectral and Sentinel-2 data using a generative adversarial network. Remote Sens. Environ. 270, 112885.

Chen, J., Sasaki, J., 2021. Mapping of subtidal and intertidal seagrass meadows via application of the feature pyramid network to unmanned aerial vehicle orthophotos. Remote Sens. 13 (23).

Christophe, E., Michel, J., Inglada, J., 2011. Remote sensing processing: from multicore to GPU. IEEE J.Select.Top.Appl.Earth Observ.Remote Sens. 4 (3), 643–652.

Coffer, M.M., Schaeffer, B.A., Zimmerman, R.C., Hill, V., Li, J., Islam, K.A., Whitman, P. J., 2020. Performance across WorldView-2 and RapidEye for reproducible seagrass mapping. Remote Sens. Environ. 250.

Csillik, O., Kumar, P., Mascaro, J., O'Shea, T., Asner, G.P., 2019. Monitoring tropical forest carbon stocks and emissions using Planet satellite data. Sci. Rep. 9 (1).

Darmawan, S., Sari, D.K., Takeuchi, W., Wikantika, K., Hernawati, R., 2019. Development of aboveground mangrove forests' biomass dataset for Southeast Asia based on ALOS-PALSAR 25-m mosaic. J. Appl. Remote. Sens. 13 (4), 1–15, 15.

Dierssen, H.M., Zimmerman, R.C., Drake, L.A., Burdige, D., 2010. Benthic ecology from space: optics and net primary production in seagrass and benthic algae across the Great Bahama Bank. Mar. Ecol. Prog. Ser. 411, 1–15.

Donato, D.C., Kauffman, J.B., Murdiyarso, D., Kurnianto, S., Stidham, M., Kanninen, M., 2011. Mangroves among the most carbon-rich forests in the tropics. Nat. Geosci. 4 (5), 293–297.

Drusch, M., Del Bello, U., Carlier, S., Colin, O., Fernandez, V., Gascon, F., Hoersch, B., Isola, C., Laberinti, P., Martimort, P., Meygret, A., Spoto, F., Sy, O., Marchese, F., Bargellini, P., 2012. Sentinel-2: ESA's optical high-resolution mission for GMES operational services. Remote Sens. Environ. 120, 25–36.

Dube, T., Mutanga, O., 2015. Quantifying the variability and allocation patterns of aboveground carbon stocks across plantation forest types, structural attributes and age in sub-tropical coastal region of KwaZulu Natal, South Africa using remote sensing. Appl. Geogr. 64, 55–65.

Dunic, J.C., Brown, C.J., Connolly, R.M., Turschwell, M.P., Côté, I.M., 2021. Long-term declines and recovery of meadow area across the world's seagrass bioregions. Glob. Chang. Biol. 27 (17), 4096–4109.

Duong, P.C., Trung, T.H., Nasahara, K.N., Tadono, T., 2018. JAXA high-resolution land use/land cover map for Central Vietnam in 2007 and 2017. Remote Sens. 10 (9).

Eck, C., 2001. Navigation algorithms with applications to unmanned helicopters, 205-205.

Effiom, A.E., van Leeuwen, L.M., Nyktas, P., Okojie, J.A., Erdbrügger, J., 2019. Combining unmanned aerial vehicle and multispectral Pleiades data for tree species identification, a prerequisite for accurate carbon estimation. J. Appl. Remote. Sens. 13 (03), 1.

Eisenbeiss, H., 2004. A mini unmanned aerial vehicle (UAV): system overview and image acquisition. In: Proceedings of the International Workshop on Processing and Visualization using High-Resolution Imagery: 1-7..

Englhart, S., Keuck, V., Siegert, F., 2011. Aboveground biomass retrieval in tropical forests - the potential of combined X- and L-band SAR data use. Remote Sens. Environ. 115 (5), 1260–1271.

Farzanmanesh, R., Khoshelham, K., Thomas, S., 2021. Technological opportunities for measuring and monitoring blue carbon initiatives in mangrove ecosystems. Remote Sens.Appl. Soc. Environ. 24, 100612.

Feliciano, E.A., Wdowinski, S., Potts, M.D., Lee, S.-K., Fatoyinbo, T.E., 2017. Estimating mangrove canopy height and above-ground biomass in the everglades national park with airborne LiDAR and TanDEM-X data. Remote Sens. 9 (7), 702.

Feng, L., Chen, S., Zhang, C., Zhang, Y., He, Y., 2021. A comprehensive review on recent applications of unmanned aerial vehicle remote sensing with various sensors for high-throughput plant phenotyping. Comput. Electron. Agric. 182.

Fernandes, M.R., Aguiar, F.C., Martins, M.J., Rico, N., Ferreira, M.T., Correia, A.C., 2020. Carbon stock estimations in a mediterranean riparian forest: a case study combining field data and UAV imagery. Forests 11 (4).

Fourqurean, J.W., Duarte, C.M., Kennedy, H., Marbà, N., Holmer, M., Mateo, M.A., Apostolaki, E.T., Kendrick, G.A., Krause-Jensen, D., McGlathery, K.J., Serrano, O., 2012. Seagrass ecosystems as a globally significant carbon stock. Nat. Geosci. 5 (7), 505–509.

Franklin, J., Miller, J.A., 2010. Mapping species distributions: Spatial inference and prediction, 1-320 pp.

Friess, D.A., Moller, I., Spencer, T., Smith, G.M., Thomson, A.G., Hill, R.A., 2014. Coastal saltmarsh managed realignment drives rapid breach inlet and creek evolution, Freiston Shore (UK). Geomorphology 208, 22–33.

Friess, D.A., Rogers, K., Lovelock, C.E., Krauss, K.W., Hamilton, S.E., Lee, S.Y., Lucas, R., Primavera, J., Rajkaran, A., Shi, S., 2019. The state of the world's mangrove forests: past, present, and Future. Annu. Rev. Environ. Resour. 44 (1), 89–115.

Ghamisi, P., Yokoya, N., Li, J., Liao, W., Liu, S., Plaza, J., Rasti, B., Plaza, A., 2017. Advances in hyperspectral image and signal processing: a comprehensive overview of the state of the art. IEEE Geosci.Remote Sens.Mag. 5 (4), 37–78.

Ghorbanian, A., Zaghian, S., Asiyabi, R.M., Amani, M., Mohammadzadeh, A., Jamali, S., 2021. Mangrove ecosystem mapping using Sentinel-1 and Sentinel-2 satellite images and random forest algorithm in Google Earth Engine. Remote Sens. 13 (13), 2565.

Gholizadeh, A., Kopačková, V., 2019. Detecting vegetation stress as a soil contamination proxy: a review of optical proximal and remote sensing techniques. Int. J. Environ. Sci. Technol. 16 (5), 2511–2524.

Ha, N.-T., Pham, T.-D., Pham, H.-T., Tran, D.-A., Hawes, I., 2023. Total organic carbon estimation in seagrass beds in Tauranga Harbour, New Zealand using multi-sensors imagery and grey wolf optimization. Geocarto Int. 38 (1), 2160832.

Ha, N.T., et al., 2020. A Comparative Assessment of Ensemble-Based Machine Learning and Maximum Likelihood Methods for Mapping Seagrass Using Sentinel-2 Imagery in Tauranga Harbor, New Zealand. Remote Sens. 12 (3), 355. https://doi.org/10.3390/rs12030355.

Ha, N.-T., Manley-Harris, M., Pham, T.-D., Hawes, I., 2021a. Detecting multi-decadal changes in seagrass cover in Tauranga Harbour, New Zealand, using Landsat imagery and boosting ensemble classification techniques. ISPRS Int. J. Geo Inf. 10 (6), 371.

Ha, N.T., Manley-Harris, M., Pham, T.D., Hawes, I., 2021. The use of radar and optical satellite imagery combined with advanced machine learning and metaheuristic optimization techniques to detect and quantify above ground biomass of intertidal seagrass in a New Zealand estuary, 42 (12), 4716–4742. https://doi.org/10.1080/01431161.2021.1899335.

Hagen, N., Kudenov, M.W., 2013. Review of snapshot spectral imaging technologies. Opt. Eng. 52 (9), 090901-090901.

Hamilton, S.E., Friess, D.A., 2018. Global carbon stocks and potential emissions due to mangrove deforestation from 2000 to 2012. Nat. Clim. Chang. 8 (3), 240–244.

Harmel, T., Chami, M., Tormos, T., Reynaud, N., Danis, P.-A., 2018. Sunglint correction of the Multi-Spectral Instrument (MSI)-SENTINEL-2 imagery over inland and sea waters from SWIR bands. Remote Sens. Environ. 204, 308–321.

Hedley, J.D., Roelfsema, C.M., Phinn, S.R., Mumby, P.J., 2012. Environmental and sensor limitations in optical remote sensing of coral reefs: implications for monitoring and sensor design. Remote Sens. 4 (1), 271–302.

Hickey, S.M., Callow, N.J., Phinn, S., Lovelock, C.E., Duarte, C.M., 2018. Spatial complexities in aboveground carbon stocks of a semi-arid mangrove community: a remote sensing height-biomass-carbon approach. Estuar. Coast. Shelf Sci. 200, 194–201.

Hill, V.J., Zimmerman, R.C., Bissett, W.P., Dierssen, H., Kohler, D.D.R., 2014. Evaluating light availability, seagrass biomass, and productivity using hyperspectral airborne remote sensing in Saint Joseph's Bay, Florida. Estuar.Coasts 37 (6), 1467–1489.

Hong, D., Yokoya, N., Xia, G.-S., Chanussot, J., Zhu, X.X., 2020. X-ModalNet: a semi-supervised deep cross-modal network for classification of remote sensing data. ISPRS J. Photogramm. Remote Sens. 167, 12–23.

Hong, D., Gao, L., Yokoya, N., Yao, J., Chanussot, J., Du, Q., Zhang, B., 2021. More diverse means better: multimodal deep learning meets remote-sensing imagery classification. IEEE Trans. Geosci. Remote Sens. 59 (5), 4340–4354.

Howard, J., Hoyt, S., Isensee, K., Telszewski, M., Pidgeon, E. (Eds.), 2014. Coastal blue carbon: methods for assessing carbon stocks and emissions factors in mangroves, tidal salt marshes, and seagrasses. Conservation International, Intergovernmental Oceanographic Commission of UNESCO, International Union for Conservation of Nature, Arlington, VA, USA, 180p.

Hu, F., Xia, G.-S., Hu, J., Zhang, L., 2015. Transferring deep convolutional neural networks for the scene classification of high-resolution remote sensing imagery. Remote Sens. 7 (11), 14680–14707.

Hu, L., Xu, N., Liang, J., Li, Z., Chen, L., Zhao, F., 2020. Advancing the mapping of mangrove forests at national-scale using Sentinel-1 and Sentinel-2 time-series data with Google Earth Engine: a Case study in China. Remote Sens. 12 (19), 3120.

Hudak, A.T., Strand, E.K., Vierling, L.A., Byrne, J.C., Eitel, J.U.H., Martinuzzi, S., Falkowski, M.J., 2012. Quantifying aboveground forest carbon pools and fluxes from repeat LiDAR surveys. Remote Sens. Environ. 123, 25–40.

Hughes, L.H., Marcos, D., Lobry, S., Tuia, D., Schmitt, M., 2020. A deep learning framework for matching of SAR and optical imagery. ISPRS J. Photogramm. Remote Sens. 169, 166–179.

Ilori, C.O., Pahlevan, N., Knudby, A., 2019. Analyzing performances of different atmospheric correction techniques for Landsat 8: application for coastal remote sensing. Remote Sens. 11 (4), 469.

Isnaen, Z., Pratama, A.P., Utami, A.A., Prananda, A.R.A., Purnama, A.D., Zhafarina, Z., Wicaksono, P., 2019. Carbon stock estimation of seagrass species thalassia hempricii using planet imagery with band ratio transformation in nirwana beach, Padang city. IOP Conference Series: Earth and Environmental Science 280 (1), 012039.

Jayathilake, D.R.M., Costello, M.J., 2018. A modelled global distribution of the seagrass biome. Biol. Conserv. 226, 120–126.

Jensen, J.R., 1996. Introductory Digital Image Processing: A Remote Sensing Perspective. Prentice-Hall Inc, Saddle River, New York.

Jones, A.R., Raja Segaran, R., Clarke, K.D., Waycott, M., Goh, W.S.H., Gillanders, B.M., 2020. Estimating mangrove tree biomass and carbon content: a comparison of forest inventory techniques and drone imagery. Frontiers in MarineScience 6.

Keogh, E., Mueen, A., 2010. Curse of dimensionality. In: Sammut, C., Webb, G.I. (Eds.), Encyclopedia of Machine Learning. Springer, US, Boston, MA, pp. 257–258.

Kellenberger, B., Marcos, D., Lobry, S., Tuia, D., 2019. Half a percent of labels is enough: efficient animal detection in UAV imagery using deep CNNs and active learning. IEEE Trans. Geosci. Remote Sens. 57 (12), 9524–9533.

Kellenberger, B., Tuia, D., Morris, D., 2020. AIDE: Accelerating image-based ecological surveys with interactive machine learning. Methods Ecol. Evol. 11 (12), 1716–1727.

Komiyama, A., Ong, J.E., Poungparn, S., 2008. Allometry, biomass, and productivity of mangrove forests: a review. Aquat. Bot. 89 (2), 128–137.

Kulawardhana, R.W., Popescu, S.C., Feagin, R.A., 2014. Fusion of lidar and multispectral data to quantify salt marsh carbon stocks. Remote Sens. Environ. 154, 345–357.

Kumar, A., Abhishek, K., Kumar Singh, A., Nerurkar, P., Chandane, M., Bhirud, S., Patel, D., Busnel, Y., 2021. Multilabel classification of remote sensed satellite imagery. Trans. Emerg. Telecommun. Technol. 32 (7), e3988.

Kumar, D., 2021. Urban objects detection from C-band synthetic aperture radar (SAR) satellite images through simulating filter properties. Sci. Rep. 11 (1).

Ladd, Cai J.T., Smeaton, Craig, Skov, Martin W., Austin, William E.N., 2022. Best practice for upscaling soil organic carbon stocks in salt marshes. Geoderma 428, 116188. https://doi.org/10.1016/j.geoderma.2022.116188.

Lagomasino, D., Fatoyinbo, T., Lee, S., Feliciano, E., Trettin, C., Shapiro, A., Mangora, M. M., 2019. Measuring mangrove carbon loss and gain in deltas. Environ. Res. Lett. 14 (2), 025002.

Lam-Dao, N., Pham-Bach, V., Nguyen-Thanh, M., Pham-Thi, M.-T., Hoang-Phi, P., 2011. Change detection of land use and riverbank in Mekong Delta, Vietnam using time series remotely sensed data. J.Resourc.Ecol. 2 (4), 370–374.

Lary, D.J., Alavi, A.H., Gandomi, A.H., Walker, A.L., 2016. Machine learning in geosciences and remote sensing. Geosci. Front. 7 (1), 3–10.

Lausch, A., Schaepman, M.E., Skidmore, A.K., Catana, E., Bannehr, L., Bastian, O., Borg, E., Bumberger, J., Dietrich, P., Glässer, C., Hacker, J.M., Höfer, R., Jagdhuber, T., Jany, S., Jung, A., Karnieli, A., Klenke, R., Kirsten, T., Ködel, U., Kresse, W., Mallast, U., Montzka, C., Möller, M., Mollenhauer, H., Pause, M., Rahman, M., Schrodt, F., Schmullius, C., Schütze, C., Selsam, P., Syrbe, R.-U., Truckenbrodt, S., Vohland, M., Volk, M., Wellmann, T., Zacharias, S., Baatz, R., 2022. Remote Sensing of Geomorphodiversity Linked to Biodiversity—Part III: Traits, Processes and Remote Sensing Characteristics. Remote Sens. 14 (9), 2279.

Lausch, A., Schaepman, M.E., Skidmore, A.K., Truckenbrodt, S.C., Hacker, J.M., Baade, J., Bannehr, L., Borg, E., Bumberger, J., Dietrich, P., Gläßer, C., Haase, D., Heurich, M., Jagdhuber, T., Jany, S., Krönert, R., Möller, M., Mollenhauer, H., Montzka, C., Pause, M., Rogass, C., Salepci, N., Schmullius, C., Schrodt, F., Schütze, C., Schweitzer, C., Selsam, P., Spengler, D., Vohland, M., Volk, M., Weber, U., Wellmann, T., Werban, U., Zacharias, S., Thiel, C., 2020. Linking the remote sensing of geodiversity and traits relevant to biodiversity—Part II: Geomorphology,terrain and surfaces. Remote Sens. 12 (22), 3690.

Le, N.N., Pham, T.D., Yokoya, N., Ha, N.T., Nguyen, T.T.T., Tran, T.D.T., Pham, T.D., 2021. Learning from multimodal and multisensor earth observation dataset for improving estimates of mangrove soil organic carbon in Vietnam. Int. J. Remote Sens. 42 (18), 6866–6890.

Lebrasse, M.C., Schaeffer, B.A., Coffer, M.M., Peter, Whitman, J., Zimmerman, R.C., Hill, V.J., Kazi, Islam, A., Li, J., Christopher, Osburn, L., 2022. Temporal stability of seagrass extent, leaf area, and carbon storage in St. Joseph Bay, Florida: a Semi-automated remote sensing analysis. Estuaries and Coasts 1, 1–20.

Lebrasse, M.C., Schaeffer, B.A., Zimmerman, R.C., Hill, V.J., Coffer, M.M., Whitman, P.J., Salls, W.B., Graybill, D.D., Osburn, C.L., 2022. Simulated response of St. Joseph Bay, Florida, seagrass meadows and their belowground carbon to anthropogenic and climate impacts. Marine Environmental Research 179, 105694.

Li, Q., Jin, R., Ye, Z., Gu, J., Li, D., He, J., Christakos, G., Agusti, S., Duarte, C.M., Wu, J., 2022. Mapping seagrass meadows in coastal China using GEE. Geocarto Int. 1–15.

Li, Y., Li, M., Li, C., Liu, Z., 2020. Forest aboveground biomass estimation using Landsat 8 and Sentinel-1A data with machine learning algorithms. Sci. Rep. 10 (1), 9952.

Li, Y., Zhang, H., Xue, X., Jiang, Y., Shen, Q., 2018. Deep learning for remote sensing image classification: a survey. WIREs Data Mining and Knowledge Discovery 8 (6), e1264.

Li, Z., Zan, Q., Yang, Q., Zhu, D., Chen, Y., Yu, S., 2019. Remote estimation of mangrove aboveground carbon stock at the species level using a low-cost unmanned aerial vehicle system. Remote Sens. 11 (9), 1018.

Liu, L., Ji, M., Buchroithner, M., 2017. Combining partial least squares and the gradient-boosting method for soil property retrieval using visible near-infrared shortwave infrared spectra. Remote Sens. 9 (12), 1299.

Liu, L., Ji, M., Buchroithner, M., 2018. Transfer Learning for Soil Spectroscopy based on Convolutional Neural Networks and its Application in Soil Clay Content Mapping using Hyperspectral Imagery. Sensors 18 (9), 3169.

López-Serrano, P., Corral-Rivas, J., Díaz-Varela, R., Álvarez-González, J., López-Sánchez, C., 2016. Evaluation of radiometric and atmospheric correction algorithms for aboveground forest biomass estimation using Landsat 5 TM Data. Remote Sens. 8 (5), 369.

Lu, D., 2006. The potential and challenge of remote sensing-based biomass estimation. Int. J. Remote Sens. 27 (7), 1297–1328.

Luo, S., Wang, C., Xi, X., Pan, F., Qian, M., Peng, D., Nie, S., Qin, H., Lin, Y., 2017. Retrieving aboveground biomass of wetland Phragmites australis (common reed) using a combination of airborne discrete-return LiDAR and hyperspectral data. Int. J. Appl. Earth Obs. Geoinf. 58, 107–117.

Maciel, F.P., Pedocchi, F., 2022. Evaluation of ACOLITE atmospheric correction methods for Landsat-8 and Sentinel-2 in the Río de la Plata turbid coastal waters. Int. J. Remote Sens. 43 (1), 215–240.

Macreadie, P.I., Anton, A., Raven, J.A., Beaumont, N., Connolly, R.M., Friess, D.A., Kelleway, J.J., Kennedy, H., Kuwae, T., Lavery, P.S., Lovelock, C.E., Smale, D.A., Apostolaki, E.T., Atwood, T.B., Baldock, J., Bianchi, T.S., Chmura, G.L., Eyre, B.D., Fourqurean, J.W., Hall-Spencer, J.M., Huxham, M., Hendriks, I.E., Krause-Jensen, D., Laffoley, D., Luisetti, T., Marbà, N., Masque, P., McGlathery, K.J., Megonigal, J.P., Murdiyarso, D., Russell, B.D., Santos, R., Serrano, O., Silliman, B.R., Watanabe, K., Duarte, C.M., 2019. The future of Blue Carbon science. Nature Communications 10 (1), 1–13, 2019.

Macreadie, P.I., Costa, M.D.P., Atwood, T.B., Friess, D.A., Kelleway, J.J., Kennedy, H., Lovelock, C.E., Serrano, O., Duarte, C.M., 2021. Blue carbon as a natural climate solution. Nat.Rev.Earth Environ. 2 (12), 826–839.

Maeda, Y., Fukushima, A., Imai, Y., Tanahashi, Y., Nakama, E., Ohta, S., Kawazoe, K., Akune, N., 2016. Estimating carbon stock changes of mangrove forests using satellite imagery and airborne lidar data in the south Sumatra state, Indonesia. International Archives of the Photogrammetry, Remote Sensing and Spatial Information Sciences 8..

Mansfeld, J., Runia, D., 2010. In: Chapter 3 Using SAR data for Mapping Deforestation and Forest Degradation, pp. 341–350.

Malerba, M.E., de Paula, Duarte, Costa, M., Friess, D.A., Schuster, L., Young, M.A., Lagomasino, D., Serrano, O., Hickey, S.M., York, P.H., Rasheed, M., Lefcheck, J.S., Radford, B., Atwood, T.B., Ierodiaconou, D., Macreadie, P., 2023. Remote sensing for cost-effective blue carbon accounting. Earth Sci. Rev. 238, 104337.

Martins, V., Barbosa, C., de Carvalho, L., Jorge, D., Lobo, F., Novo, E., 2017. Assessment of atmospheric correction methods for Sentinel-2 MSI images applied to Amazon floodplain lakes. Remote Sens. 9 (4), 322.

Masek, J.G., Wulder, M.A., Markham, B., McCorkel, J., Crawford, C.J., Storey, J., Jenstrom, D.T., 2020. Landsat 9: Empowering open science and applications through continuity. Remote Sens. Environ. 248, 111968.

McKenzie, L.J., Nordlund, L.M., Jones, B.L., Cullen-Unsworth, L.C., Roelfsema, C., Unsworth, R.K.F., 2020. The global distribution of seagrass meadows. Environ. Res. Lett. 15 (7), 074041.

Méléder, V., Savelli, R., Barnett, A., Polsenaere, P., Gernez, P., Cugier, P., Lerouxel, A., Le Bris, A., Dupuy, C., Le Fouest, V., Lavaud, J., 2020. Mapping the intertidal microphytobenthos gross primary production part I: Coupling multispectral remote sensing and physical modeling. Front. Marine Sci 7. Front. Marine Sci., 7.

Murray, N.J., Worthington, T.A., Bunting, P., Duce, S., Hagger, V., Lovelock, C.E., Lucas, R., Saunders, M.I., Sheaves, M., Spalding, M., Waltham, N.J., Lyons, M.B., 2022. High-resolution mapping of losses and gains of Earth's tidal wetlands. Science 376 (6594), 744–749.

Nabil Akbar, M., Faizal, A., Anugrah La Nafie, Y., Werorilangi, S., Mashoreng, S., 2021. Seagrass carbon stock estimation in Panrangluhu coastal waters using remote

sensing technology. IOP Conference Series: Earth and Environmental Science 860 (1), 012085.
Neupane, B., Horanont, T., Aryal, J., 2021. Deep Learning-based semantic segmentation of urban features in satellite images: a review and meta-analysis. Remote Sens. 13 (4), 808.
Ngo, P.T.T., Pham, T.D., Nhu, V.H., Le, T.T., Tran, D.A., Phan, D.C., Hoa, P.V., Amaro-Mellado, J.L., Bui, D.T., 2021. A novel hybrid quantum-PSO and credal decision tree ensemble for tropical cyclone induced flash flood susceptibility mapping with geospatial data. J. Hydrol. 596.
Nguyen, H., Jung, J., Lee, J., Choi, S.-U., Hong, S.-Y., Heo, J., 2015. Optimal atmospheric correction for above-ground forest biomass estimation with the ETM+ remote sensor. Sensors 15 (8), 18865.
Nguyen, T.T., Pham, T.D., Nguyen, C.T., Delfos, J., Archibald, R., Dang, K.B., Hoang, N. B., Guo, W., Ngo, H.H., 2022. A novel intelligence approach based active and ensemble learning for agricultural soil organic carbon prediction using multispectral and SAR data fusion. Sci. Total Environ. 804, 150187.
Nhu, V.H., Ngo, P.T.T., Pham, T.D., Dou, J., Song, X., Hoang, N.D., Tran, D.A., Cao, D.P., Aydilek, I.B., Amiri, M., Costache, R., Hoa, P.V., Bui, D.T., 2020. A new hybrid firefly-pso optimized random subspace tree intelligence for torrential rainfall-induced flash flood susceptible mapping. Remote Sens. 12 (17).
Nickolls, J., Dally, W.J., 2010. The GPU Computing Era. IEEE Micro 30 (2), 56–69.
Omar, H., Misman, M.A., Linggok, V., 2018. Characterizing and monitoring of mangroves in Malaysia using Landsat-based spatial-spectral variability. IOP Conference Series: Earth and Environmental Science 169, 012037.
Oquab, M., Bottou, L., Laptev, I., Sivic, J., 2014. In: Learning and Transferring Mid-level Image Representations Using Convolutional Neural Networks, 2014 IEEE Conference on Computer Vision and Pattern Recognition, pp. 1717–1724, 2019.
Otero, V., Van De Kerchove, R., Satyanarayana, B., Martínez-Espinosa, C., Fisol, M.A.B., Ibrahim, M.R.B., Sulong, I., Mohd-Lokman, H., Lucas, R., Dahdouh-Guebas, F., 2018. Managing mangrove forests from the sky: Forest inventory using field data and unmanned aerial vehicle (UAV) imagery in the Matang Mangrove Forest Reserve, peninsular Malaysia. For. Ecol. Manag. 411, 35–45.
Ouyang, X., Lee, S.Y., 2020. Improved estimates on global carbon stock and carbon pools in tidal wetlands. Nat.Commun. 11 (1), 1–7.
Owers, C.J., Rogers, K., Woodroffe, C.D., 2018. Terrestrial laser scanning to quantify above-ground biomass of structurally complex coastal wetland vegetation. Estuar. Coast. Shelf Sci. 204, 164–176.
Padarian, J., Minasny, B., McBratney, A.B., 2019. Transfer learning to localise a continental soil Vis-NIR calibration model. Geoderma 340, 279–288.
Pajares, G., 2015. Overview and current status of remote sensing applications based on unmanned aerial vehicles (UAVs). Photogramm. Eng. Remote. Sens. 81 (4), 281–329.
Pan, S.J., Yang, Q., 2010. A survey on transfer learning. IEEE Trans. Knowl. Data Eng. 22 (10), 1345–1359.
Pancorbo, J.L., Lamb, B.T., Quemada, M., Hively, W.D., Gonzalez-Fernandez, I., Molina, I., 2021. Sentinel-2 and WorldView-3 atmospheric correction and signal normalization based on ground-truth spectroradiometric measurements. ISPRS J. Photogramm. Remote Sens. 173, 166–180.
Pandey, P.C., Anand, A., Srivastava, P.K., 2019. Spatial distribution of mangrove forest species and biomass assessment using field inventory and earth observation hyperspectral data. Biodivers. Conserv. 28 (8), 2143–2162.
Painam, R.K., Manikandan, S., 2021. A comprehensive review of SAR image filtering techniques: systematic survey and future directions. Arab. J. Geosci. 14 (1), 37.
Pereira-Sandoval, M., Ruescas, A., Urrego, P., Ruiz-Verdú, A., Delegido, J., Tenjo, C., Soria-Perpinyà, X., Vicente, E., Soria, J., Moreno, J., 2019. Evaluation of atmospheric correction algorithms over Spanish inland waters for Sentinel-2 multi spectral imagery data. Remote Sens. 11 (12), 1469.
Pham, L.T.H., Brabyn, L., 2017. Monitoring mangrove biomass change in Vietnam using SPOT images and an object-based approach combined with machine learning algorithms. ISPRS J. Photogramm. Remote Sens. 128, 86–97.
Pham, T.D., Le, N.N., Ha, N.T., Nguyen, L.V., Xia, J., Yokoya, N., To, T.T., Trinh, H.X., Kieu, L.Q., Takeuchi, W., 2020a. Estimating mangrove above-ground biomass using extreme gradient boosting decision trees algorithm with fused Sentinel-2 and ALOS-2 PALSAR-2 data in Can Gio Biosphere Reserve,Vietnam. Remote Sensing 12 (5), 777.
Pham, T.D., Xia, J., Ha, N.T., Bui, D.T., Le, N.N., Takeuchi, W., 2019a. A review of remote sensing approaches for monitoring blue carbon ecosystems: mangroves, seagrasses and salt marshes during 2010–2018. Sensors 19 (8), 1933.
Pham, T.D., Yokoya, N., Bui, D.T., Yoshino, K., Friess, D.A., 2019b. Remote sensing approaches for monitoring mangrove species, structure, and biomass: opportunities and challenges. Remote Sens. 11 (3), 230.
Pham, T.D., Yokoya, N., Nguyen, T.T.T., Le, N.N., Ha, N.T., Xia, J., Takeuchi, W., Pham, T.D., 2021. Improvement of mangrove soil carbon stocks estimation in North Vietnam using Sentinel-2 data and machine learning approach. GIScience Remote Sens. 58 (1), 68–87.
Pham, T.D., Yokoya, N., Xia, J., Ha, N.T., Le, N.N., Nguyen, T.T.T., Dao, T.H., Vu, T.T.P., Pham, T.D., Takeuchi, W., 2020b. Comparison of machine learning methods for estimating mangrove above-ground biomass using multiple source remote sensing data in the Red River Delta Biosphere Reserve,Vietnam. Remote Sens. 12 (8), 1334.
Pham, T.D., Yoshino, K., 2017. Aboveground biomass estimation of mangrove species using ALOS-2 PALSAR imagery in Hai Phong City, Vietnam. J.Appl.Remote Sens. 11 (2), 026010.
Pham, T.D., Yoshino, K., Bui, D.T., 2017. Biomass estimation of Sonneratia caseolaris (l.) Engler at a coastal area of Hai Phong city (Vietnam) using ALOS-2 PALSAR imagery and GIS-based multi-layer perceptron neural networks. GIScience Remote Sens. 54 (3), 329–353.
Pham, T.D., Yoshino, K., Le, N., Bui, D., 2018. Estimating aboveground biomass of a mangrove plantation on the Northern coast of Vietnam using machine learning techniques with an integration of ALOS-2 PALSAR-2 and Sentinel-2A data. Int. J. Remote Sens. 39 (22), 7761–7788.
Phan, D.C., Trung, T.H., Truong, V.T., Nasahara, K.N., 2021a. Ensemble learning updating classifier for accurate land cover assessment in tropical cloudy areas. Geocarto Int. 1–18.
Phan, D.C., Trung, T.H., Truong, V.T., Sasagawa, T., Vu, T.P.T., Bui, D.T., Hayashi, M., Tadono, T., Nasahara, K.N., 2021b. First comprehensive quantification of annual land use/cover from 1990 to 2020 across mainland Vietnam. Sci. Rep. 11 (1).
Pires de Lima, R., Marfurt, K., 2020. Convolutional neural network for remote-sensing scene classification: transfer learning analysis. Remote Sens. 12 (1), 86.
Politi, E., Paterson, S.K., Scarrott, R., Tuohy, E., O'Mahony, C., Cámaro-García, W.C.A., 2019. Earth observation applications for coastal sustainability: potential and challenges for implementation. Anthropocene Coasts 2 (1), 306–329.
Pons, X., Pesquer, L., Cristóbal, J., González-Guerrero, O., 2014. Automatic and improved radiometric correction of Landsat imagery using reference values from MODIS surface reflectance images. Int. J. Appl. Earth Obs. Geoinf. 33, 243–254.
Potapov, P., Li, X., Hernandez-Serna, A., Tyukavina, A., Hansen, M.C., Kommareddy, A., Pickens, A., Turubanova, S., Tang, H., Silva, C.E., Armston, J., Dubayah, R., Blair, J. B., Hofton, M., 2021. Mapping global forest canopy height through integration of GEDI and Landsat data. Remote Sens. Environ. 253, 112165.
Prahalad, V., Kirkpatrick, J.B., Aalders, J., Carver, S., Ellison, J., Harrison-Day, V., McQuillan, P., Morrison, B., Richardson, A., Woehler, E., 2020. Conservation ecology of Tasmanian coastal saltmarshes, south-East Australia – a review. Pac. Conserv. Biol. 26 (2), 105–129.
Qin, R., Liu, T., 2022. A review of landcover classification with very-high resolution remotely sensed optical images; analysis unit, model scalability and transferability. Remote Sens. 14 (3), 646.
Qin, R., Tian, J., Reinartz, P., 2016. 3D change detection – approaches and applications. ISPRS J.Photogramm.Remote Sens. 122, 41–56.
Qiu, F., Berglund, J., Jensen, J.R., Thakkar, P., Ren, D., 2004. Speckle noise reduction in SAR imagery using a local adaptive median filter. GIScience Remote Sens. 41 (3), 244–266.
Rijal, S.S., Pham, T.D., Noer'Aulia, S., Putera, M.I., Saintilan, N., 2023. Mapping mangrove above-ground carbon using multi-source remote sensing data and machine learning approach in Loh Buaya, Komodo National Park, Indonesia. Forests 14 (1), 94.
Rasel, S.M.M., Chang, H.-C., Ralph, T.J., Saintilan, N., Diti, I.J., 2019. Application of feature selection methods and machine learning algorithms for saltmarsh biomass estimation using Worldview-2 imagery. Geocarto Int. 1–25.
Richards, D.R., Thompson, B.S., Wijedasa, L., 2020. Quantifying net loss of global mangrove carbon stocks from 20 years of land cover change. Nat.Commun. 11 (1), 1–7.
Rogers, K., Krauss, K.W., 2019. Moving from generalisations to specificity about mangrove –saltmarsh dynamics. Wetlands 39 (6), 1155–1178.
Saintilan, N., Wilson, N.C., Rogers, K., Rajkaran, A., Krauss, K.W., 2014. Mangrove expansion and salt marsh decline at mangrove poleward limits. Glob. Chang. Biol. 20 (1), 147–157.
Sánchez, S., Ramalho, R., Sousa, L., Plaza, A., 2015. Real-time implementation of remotely sensed hyperspectral image unmixing on GPUs. J. Real-Time Image Proc. 10 (3), 469–483.
Sanderman, J., Hengl, T., Fiske, G., Solvik, K., Adame, M.F., Benson, L., Bukoski, J.J., Carnell, P., Cifuentes-Jara, M., Donato, D., Duncan, C., Eid, E.M., Ermgassen, P.Z., Lewis, C.J.E., Macreadie, P.I., Glass, L., Gress, S., Jardine, S.L., Jones, T.G., Nsombo, E.N., Rahman, M.M., Sanders, C.J., Spalding, M., Landis, E., 2018. A global map of mangrove forest soil carbon at 30 m spatial resolution. Environ.Res.Lett. 13 (5), 055002.
Sani, D.A., Hashim, M., Hossain, M.S., 2019. Recent advancement on estimation of blue carbon biomass using satellite-based approach. Int. J. Remote Sens. 40 (20), 7679–7715.
Sarker, I.H., 2021. Deep Learning: a comprehensive overview on techniques, taxonomy, applications and research directions. SN Computer Sci. 2 (6), 420.
Sejati, A.W., Buchori, I., Kurniawati, S., Brana, Y.C., Fariha, T.I., 2020. Quantifying the impact of industrialization on blue carbon storage in the coastal area of Metropolitan Semarang,Indonesia. Appl. Geogr. 124, 102319.
Shahbazi, M., Théau, J., Ménard, P., 2014. Recent applications of unmanned aerial imagery in natural resource management. GIScience Remote Sens. 51 (4), 339–365.
Shakhatreh, H., Sawalmeh, A.H., Al-Fuqaha, A., Dou, Z., Almaita, E., Khalil, I., Othman, N.S., Khreishah, A., Guizani, M., 2019. Unmanned aerial vehicles (UAVs): a survey on civil applications and key research challenges. IEEE Access 7, 48572–48634.
Shapiro, A.C., Trettin, C.C., Küchly, H., Alavinapanah, S., Bandeira, S., 2015. The Mangroves of the Zambezi Delta: increase in extent observed via satellite from 1994 to 2013. Remote Sens. 7 (12), 16504–16518.
Simard, M., Fatoyinbo, L., Smetanka, C., Rivera-Monroy, V.H., Castañeda-Moya, E., Thomas, N., Van der Stocken, T., 2019. Mangrove canopy height globally related to precipitation, temperature and cyclone frequency. Nat. Geosci. 12 (1), 40–45.
Simard, M., Zhang, K., Rivera-Monroy, V.H., Ross, M.S., Ruiz, P.L., Castañeda-Moya, E., Twilley, R.R., Rodriguez, E., 2006. Mapping height and biomass of mangrove forests in Everglades National Park with SRTM elevation data. Photogramm. Eng. Remote Sens. 72 (3), 299–311.
Simpson, K., Bruce, E., Davies, K.P., Barber, P., 2020. A blueprint for estimation of seagrass carbon stock using remote sensing. Remote Sens. 14 (15), 3572.
Sinha, S., Jeganathan, C., Sharma, L.K., Nathawat, M.S., 2015. A review of radar remote sensing for biomass estimation. Int. J. Environ. Sci. Technol. 12 (5), 1779–1792.

Stovall, A.E.L., Fatoyinbo, T., Thomas, N.M., Armston, J., Ebanega, M.O., Simard, M., Trettin, C., Obiang Zogo, R.V., Aken, I.A., Debina, M., Me Kemoe, A.M., Assoumou, E.O., Kim, J.S., Lagomasino, D., Lee, S.-K., Ndong Obame, J.C., Voubou, G.D., Essono, C.Z., 2021. Comprehensive comparison of airborne and spaceborne SAR and LiDAR estimates of forest structure in the tallest mangrove forest on earth. Sci.Remote Sens. 4, 100034.

Suyadi, Gao, J., Lundquist, C.J., Schwendenmann, L., 2020. Aboveground carbon stocks in rapidly expanding mangroves in New Zealand: regional assessment and economic valuation of blue carbon. Estuaries and Coasts 43 (6), 1456–1469.

Tang, Y.-N., Ma, J., Xu, J.-X., Wu, W.-B., Wang, Y.-C., Guo, H.-Q., 2022. Assessing the impacts of tidal creeks on the spatial patterns of coastal salt marsh vegetation and its aboveground biomass. Remote Sens. 14 (8), 1839.

Tang, W., Feng, W., Jia, M., Shi, J., Zuo, H., Trettin, C.C., 2015. The assessment of mangrove biomass and carbon in West Africa: a spatially explicit analytical framework. Wetlands Ecol.Manag. 24 (2), 153–171.

Tang, W., Zheng, M., Zhao, X., Shi, J., Yang, J., Trettin, C.C., 2018. Big. Sustainability 10 (2), 472.

Thomas, N., Lucas, R., Itoh, T., Simard, M., Fatoyinbo, L., Bunting, P., Rosenqvist, A., 2015. An approach to monitoring mangrove extents through time-series comparison of JERS-1 SAR and ALOS PALSAR data. Wetl. Ecol. Manag. 23 (1), 3–17.

Torti, E., Danese, G., Leporati, F., Plaza, A., 2016. A hybrid CPU–GPU real-time hyperspectral unmixing chain. IEEE J.Select.Top.Appl.Earth Observ.Remote Sens. 9 (2), 945–951.

Touzi, R., Shimada, M., Motohka, T., 2022. Calibration and validation of polarimetric ALOS2-PALSAR2. Remote Sens. 14 (10), 2452.

Traganos, D., Aggarwal, B., Poursanidis, D., Topouzelis, K., Chrysoulakis, N., Reinartz, P., 2018. Towards global-scale seagrass mapping and monitoring using Sentinel-2 on Google Earth Engine: the case study of the Aegean and Ionian seas. Remote Sens. 10 (8), 1227.

Traganos, D., Pertiwi, A.P., Lee, C.B., Blume, A., Poursanidis, D., Shapiro, A., 2022. Earth observation for ecosystem accounting: spatially explicit national seagrass extent and carbon stock in Kenya, Tanzania, Mozambique and Madagascar. Remote Sens.Ecol. Conserv. 8 (6), 778–792.

Transon, J., D'Andrimont, R., Maugnard, A., Defourny, P., 2018. Survey of hyperspectral earth observation applications from space in the Sentinel-2 context. Remote Sens. 10 (2), 157.

Trettin, C.C., Dai, Z., Tang, W., Lagomasino, D., Thomas, N., Lee, S.K., Simard, M., Ebanega, M.O., Stoval, A., Fatoyinbo, T.E., 2021. Mangrove carbon stocks in Pongara National Park, Gabon. Estuar. Coast. Shelf Sci. 259, 107432.

Truong, V.T., Hoang, T.T., Cao, D.P., Hayashi, M., Tadono, T., Nasahara, K.N., 2019. JAXA annual forest cover maps for Vietnam during 2015–2018 using ALOS-2/PALSAR-2 and auxiliary data. Remote Sens. 11 (20).

Unsworth, R.K.F., McKenzie, L.J., Collier, C.J., Cullen-Unsworth, L.C., Duarte, C.M., Eklöf, J.S., Jarvis, J.C., Jones, B.L., Nordlund, L.M., 2019. Global challenges for seagrass conservation. Ambio 48 (8), 801–815.

Veettil, B.K., Ward, R.D., Lima, M.D.A.C., Stankovic, M., Hoai, P.N., Quang, N.X., 2020. Opportunities for seagrass research derived from remote sensing: a review of current methods. Ecol. Indic. 117, 106560.

Verrelst, J., Muñoz, J., Alonso, L., Delegido, J., Rivera, J.P., Camps-Valls, G., Moreno, J., 2012. Machine learning regression algorithms for biophysical parameter retrieval: opportunities for Sentinel-2 and-3. Remote Sens. Environ. 118, 127–139.

Vu, T.T.P., Pham, T.D., Saintilan, N., Skidmore, A., Luu, H.V., Vu, Q.H., Le, N.N., Nguyen, H.Q., Matsushita, B., 2022. Mapping multi-decadal mangrove extent in the Northern Coast of Vietnam using Landsat time-series data on Google Earth Engine platform. Remote Sens. 14 (18), 4664.

Wang, X., Xiao, X., Zou, Z., Hou, L., Qin, Y., Dong, J., Doughty, R.B., Chen, B., Zhang, X., Chen, Y., Ma, J., Zhao, B., Li, B., 2020. Mapping coastal wetlands of China using time series Landsat images in 2018 and Google Earth Engine. ISPRS J. Photogramm. Remote Sens. 163, 312–326.

Wannasiri, W., Nagai, M., Honda, K., Santitamnont, P., Miphokasap, P., 2013. Extraction of mangrove biophysical parameters using airborne LiDAR. Remote Sens. 5 (4), 1787–1808.

Warren, M.A., Simis, S.G.H., Martinez-Vicente, V., Poser, K., Bresciani, M., Alikas, K., Spyrakos, E., Giardino, C., Ansper, A., 2019. Assessment of atmospheric correction algorithms for the Sentinel-2A MultiSpectral Imager over coastal and inland waters. Remote Sens. Environ. 225, 267–289.

Warwick-Champion, E., Davies, K.P., Barber, P., Hardy, N., Bruce, E., 2022. Characterising the aboveground carbon content of Saltmarsh in Jervis Bay, NSW, using ArborCam and PlanetScope. Remote Sens. 14 (8), 1782.

Wicaksono, P., 2017. Mangrove above-ground carbon stock mapping of multi-resolution passive remote-sensing systems. International Journal of Remote Sensing 38 (6), 1551–1578. https://doi.org/10.1080/01431161.2017.1283072.

Wicaksono, P., Danoedoro, P., Hartono, Nehren, U., 2016. Mangrove biomass carbon stock mapping of the Karimunjawa Islands using multispectral remote sensing. International Journal of Remote Sensing 37 (1), 26–52.

Wilson, K.L., Wong, M.C., Devred, E., 2022. Comparing Sentinel-2 and WorldView-3 imagery for coastal bottom habitat mapping in Atlantic Canada. Remote Sens. 14 (5), 1254.

Wulder, M.A., Loveland, T.R., Roy, D.P., Crawford, C.J., Masek, J.G., Woodcock, C.E., Allen, R.G., Anderson, M.C., Belward, A.S., Cohen, W.B., Dwyer, J., Erb, A., Gao, F., Griffiths, P., Helder, D., Hermosilla, T., Hipple, J.D., Hostert, P., Hughes, M.J., Huntington, J., Johnson, D.M., Kennedy, R., Kilic, A., Li, Z., Lymburner, L., McCorkel, J., Pahlevan, N., Scambos, T.A., Schaaf, C., Schott, J.R., Sheng, Y., Storey, J., Vermote, E., Vogelmann, J., White, J.C., Wynne, R.H., Zhu, Z., 2019. Current status of Landsat program, science, and applications. Remote Sens. Environ. 225, 127–147.

Xia, J., Yokoya, N., Baier, G., 2022. DML: differ-modality learning for building semantic segmentation. IEEE Trans. Geosci. Remote Sens. 60, 1–14.

Xu, Q., Hou, Z., Tokola, T., 2012. Relative radiometric correction of multi-temporal ALOS AVNIR-2 data for the estimation of forest attributes. ISPRS J. Photogramm. Remote Sens. 68, 69–78.

Yan, W.Y., Shaker, A., El-Ashmawy, N., 2015. Urban land cover classification using airborne LiDAR data: a review. Remote Sens. Environ. 158, 295–310.

Yancho, J.M.M., Jones, T.G., Gandhi, S.R., Ferster, C., Lin, A., Glass, L., 2020. The Google Earth Engine Mangrove Mapping Methodology (GEEMMM). Remote Sens. 12 (22), 3758.

Yang, J., Wang, X., Wang, R., Wang, H., 2020. Combination of convolutional neural networks and recurrent neural networks for predicting soil properties using Vis–NIR spectroscopy. Geoderma 380, 114616.

Yang, Z., Zhu, Y., Pu, Y., 2008. In: Parallel Image Processing Based on CUDA, 2008 International Conference on Computer Science and Software Engineering, pp. 198–201.

Yao, H., Qin, R., Chen, X., 2019. Unmanned aerial vehicle for remote sensing applications - a review. Remote Sens. 11 (12).

Zhang, B., Li, F., Zheng, G., Wang, Y., Tan, Z., Li, X., 2021. Developing big ocean system in support of sustainable development goals: challenges and countermeasures. Big Earth Data 5 (4), 557–575.

Zheng, Y., Takeuchi, W., 2020. Quantitative assessment and driving force analysis of mangrove forest changes in China from 1985 to 2018 by integrating optical and radar imagery. ISPRS Int. J. Geo Inf. 9 (9), 513.

Zheng, Y., Takeuchi, W., 2022. Estimating mangrove forest gross primary production by quantifying environmental stressors in the coastal area. Sci. Rep. 12 (1), 2238.

Zheng, Z., Ma, A., Zhang, L., Zhong, Y., 2021. Deep multisensor learning for missing-modality all-weather mapping. ISPRS J. Photogramm. Remote Sens. 174, 254–264.

Zhong, H., Li, Y., Jiao, L., 2011. SAR image despeckling using Bayesian nonlocal means filter with sigma preselection. IEEE Geosci. Remote Sens. Lett. 8 (4), 809–813.

Zhu, H.M., Zhong, W.Q., Jiao, L.C., 2013. Combination of target detection and block-matching 3D filter for despeckling SAR images. Electron. Lett. 49 (7), 495–497.

Zhu, Y., Liu, K., Liu, L., Wang, S., Liu, H., 2015. Retrieval of mangrove aboveground biomass at the individual species level with WorldView-2 images. Remote Sens. 7 (9), 12192.